



Article

Multivariate Regression Modeling for Coastal Urban Air Quality Estimates

Soo-Min Choi ¹, Hyo Choi ^{2,*} and Woojin Paik ¹

¹ Department of Computer Engineering, Konkuk University, Chungju 27478, Republic of Korea; fuledoc@daum.net (S.-M.C.); wjpaik@kku.ac.kr (W.P.)

² Atmospheric and Oceanic Disaster Research Institute, Gangneung 25563, Republic of Korea

* Correspondence: du8392@hanmail.net; Tel.: +82-10-7240-0357

Abstract: Multivariate regression models for real-time coastal air quality forecasting were suggested from 18 to 27 March 2015, with a total of 15 kinds of hourly input data (three-hours-earlier data of PM and gas with meteorological parameters from Kangnung (Korea), associated with two-days-earlier data of PM and gas from Beijing (China)). Multiple correlation coefficients between the predicted and measured PM₁₀, PM_{2.5}, NO₂, SO₂, CO and O₃ concentrations were 0.957, 0.906, 0.886, 0.795, 0.864 and 0.932 before the yellow sand event at Kangnung, 0.936, 0.982, 0.866, 0.917, 0.887 and 0.916 during the event and 0.919, 0.945, 0.902, 0.857, 0.887 and 0.892 after the event. As the significance levels (*p*) from multi-regression analyses were less than 0.001, all correlation coefficients were very significant. Partial correlation coefficients presenting the contribution of 15 input variables to 6 output variables using the models were presented for the three periods in detail. Scatter plots and their hourly distributions between the predicted and measured values showed the quite good accuracy of the modeling performance for the current time forecasting of six output values and their high applicability.

Keywords: air quality estimate; multivariate regression modeling; PM₁₀; PM_{2.5}; NO₂; SO₂; CO; O₃; yellow sand event; significance level; partial correlation coefficient



Citation: Choi, S.-M.; Choi, H.; Paik, W. Multivariate Regression Modeling for Coastal Urban Air Quality Estimates. *Appl. Sci.* **2023**, *13*, 10556. <https://doi.org/10.3390/app131910556>

Academic Editor: Dikaia E. Saraga

Received: 27 August 2023

Revised: 17 September 2023

Accepted: 18 September 2023

Published: 22 September 2023



Copyright: © 2023 by the authors. Licensee MDPI, Basel, Switzerland. This article is an open access article distributed under the terms and conditions of the Creative Commons Attribution (CC BY) license (<https://creativecommons.org/licenses/by/4.0/>).

1. Introduction

The rapidly increasing consumption of fossil fuels, such as gasoline and coal, due to industrial development in each country and rural urbanization in northeast and southeast Asia results in worse ambient air pollution, which is mainly composed of particulate matter and gases emitted from the vehicles on the road, industries, forest fires, heating and cooking boilers, trash burning and the yellow dust raised from the desert and arid areas [1–6]. Various pollutants are very harmful to human health through respiratory diseases, are a multi-faceted health threat to outdoor physical activity and cause worse visibility during long hazy weather [7–12].

Sun et al. [13], Darmenova et al. [14], Wang et al. [15], Uno et al. [16] and Choi and Zhang [17] insist that yellow dust, which is also called various names such as Asian dust, dust storm, yellow sand and KOSA is easily caused under a relative humidity of less than 40% near the ground surface of wide arid areas and the desert in northern China and a wind velocity of over 10 m/s for the dust mobilization in spring.

Iwasaka et al. [18] carried out lidar observation to investigate the large depolarization ratio of free tropospheric aerosols over the Taklamakan Desert. Gao et al. [19], Sun [20], Chung et al. [21] and Zhang et al. [22] reported on dust storm frequency in spring and dust deposition on the Chinese Loess Plateau. As a strong northwesterly wind could remove several hundred thousand tons of both sand and dust from the desert and arid areas and those substances were uplifted, about 50% of the dust was accumulated in the desert area's vicinity and the rest was transported to downwind areas such as Korea and deposited

to its ground surface, causing low visibility due to a higher PM concentration [23,24]. Shim et al. [25] insisted that Asian dust particles transported concurrently with anthropogenic pollutants contributed to an elevated PM_{2.5} concentration, through aerosol lidar and optical particle counter measurements.

Using numerical models, Lin [26] showed the transport of yellow sand to Taiwan and Uno et al. [27] explained the long-range transport of soil dust from Asia to the tropical North Pacific. Chin et al. [28], Jaffe et al. [29] and McKendry et al. [30] indicated the long-range transport of air pollutants and Asian dust to southern California and western Canada and further analyzed the chemical composition of aerosols.

Many researchers have conducted statistical and artificial neural network modeling research to predict dust concentrations. The previous statistical analyses on the impact of yellow dust in Korea comprised simple regression models. Lee and Chung [31] explained the fractional ratio and correlations of temporal PM₁₀, PM_{2.5} and PM₁ at Gangneung that was affected by the transported dust from the Gobi Desert. Bhaskar and Mehta [32] showed the meteorological effect on particulate matters (PM) in Ahmedabad. Similarly, Chung et al. [33], Li et al. [34], Shi et al. [35] and Zhao [36] explained the relationship of PM with meteorological elements in China using multiple regression models without a gas effect.

Kim [37], Lim [38], Choi [39] and Jeon and Son [40] performed air quality prediction using artificial neural network and multivariate regression models in Korea. The predictions by two models with numerical models were very accurate. Instead of a complicated numerical model, a multivariate regression model was devised for real-time prediction of PM₁₀, PM_{2.5}, NO₂, SO₂, O₃ and CO at Kangnung (Korea), using 3 h-earlier pollution and meteorological data and 2-days-earlier pollution data from Beijing (China).

2. Study Area and Data Analysis

2.1. Study Area

Figure 1 indicates the geographical features of northeastern Asia including Russia, Mongolia (the Gobi Desert), China and Korea.



Figure 1. Geographical map of northeastern Asia with the Gobi Desert in southern Mongolia (big square) and Beijing (China; red star) and Kangnung (Korea; red circle) cities.

In spring, when the prevailing northwesterly wind blows over the deserts and arid areas in southern Mongolia and northern China, several hundred thousand tons of sand and dust could be raised up and transported downwind in an eastward direction toward Beijing (China). The dust could combine with local pollutants emitted from Beijing and

reach Korea's eastern coast, including Kangnung City, resulting in a worse influence on its urban air quality.

2.2. Measured Material and Analysis of Data

Hourly averaged PM₁₀, PM_{2.5}, SO₂, CO, O₃ and NO₂ concentrations measured at the Ockcheondong observation point of Kangnung city were obtained from the homepage (Air Korea) of the Korea Environment Corporation (website address: <https://www.airkorea.or.kr/web/>, accessed on 1 February 2023) and hourly meteorological data (air temperature (°C; TEMP), wind speed (m/s; WIND) and relative humidity (%; RH)) measured at the Okcheondong observation point of Kangnung city by the Gangwon Regional Meteorological Administration (GRMA) were obtained through a website (<https://data.kma.go.kr/>, accessed on 1 February 2023). Hourly PM₁₀, PM_{2.5}, SO₂, CO, O₃ and NO₂ values measured at the Yongdingmen observation point in Beijing, China, were also obtained (<https://quotsoft.net/air/>, accessed on 20 January 2021).

Uno et al. [16], Choi and Zhang [17] and Kai et al. [18] explained clearly that the yellow dust particles raised from the Gobi Desert under strong northwesterly wind over 10 m/s were transported toward downwind regions such as Beijing and they further combined with local pollutants emitted from the cities. Then, those particles moved to the further downwind regions such as the Korean peninsula including Kangnung city and the islands of Japan. It takes approximately two days (i.e., 48 h) for the particles to travel the over 1400 km distance between Beijing and Kangnung. This means the current concentrations of particulate matter and gases at Kangnung City should be affected by the two-days-earlier air pollutant concentrations in Beijing.

Thus, in this study to make current-time predictions of air pollutant concentrations, such as PM (PM₁₀ and PM_{2.5}) and gas (SO₂, CO, O₃ and NO₂), at Kangnung City, we used input data sets of not only three-hours-earlier data of PM, gas and meteorological parameters (air temperature, wind speed and relative humidity) at Kangnung city but also two-days-earlier data of PM and gas in Beijing.

The correlation coefficients and regression equations between the observed and predicted PM₁₀, PM_{2.5}, SO₂, CO, O₃ and NO₂ concentrations at Kangnung City affected by the PM and gases from Beijing city (China) in the yellow sand route between 18 and 27 March were divided into three periods: before the inflow of yellow dust (00:00 LST, 18 March 2015–00:00 LST 21 March 2015), during its inflow (01:00 LST, 21 March 2015–00:00 LST, 23 March 2015) and after its inflow (01:00 LST, 23 March 2015–00:00 LST, 27 March 2015). Thus, multivariate regression prediction models were obtained via multiple regression analyses using SPSS-v27 statistical software. The predicted value of each pollutant was compared with the one later observed to test the goodness of its predicted value.

3. Results

3.1. Satellite Images of Yellow Dust Transport

We used GONE-2 (METOP-B) KNMI/O3MSAF/EUMETSAT satellite images reflecting a cloud of dust before and during yellow sand periods in 2015 to investigate the transport of yellow dust from northern China, including desert and dry areas, to the downwind regions, such as South China, Korea and Japan, in the dust transport route in Figure 2a,b.

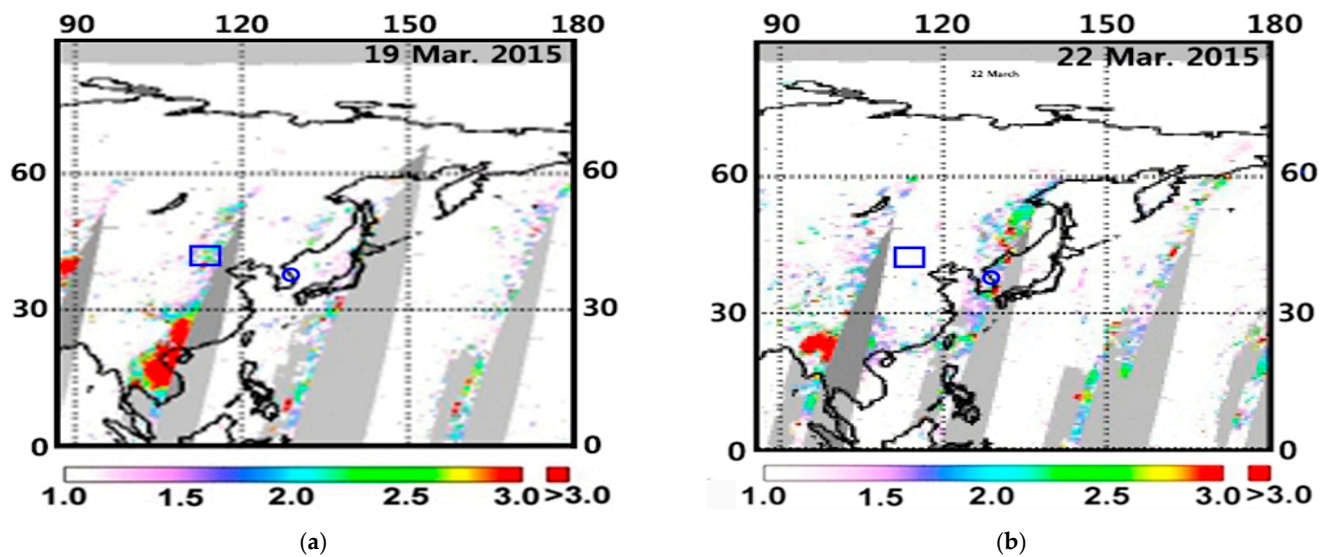


Figure 2. GONE-2 (METOP-B) KNMI/O3MSAF/EUMETSAT satellite images reflecting a cloud of dust on (a) 19 March 2015 (before) and (b) 22 March (during the period of the yellow sand event in Korea). Small blue squares and circles denote Beijing (China) and Kangnung (Korea). (<https://www.temis.nl/aviation/aai-archive.php?Year=2015&Month=03&Day=19>, accessed on 25 February 2023).

Figure 2a shows that the GONE-2 (METOP-B) satellite images can reflect the yellow sand and dust initially raised from the arid areas in the east of Lake Baikal in Siberia (Russia), the Gobi Desert and Inner Mongo in northern China. Then, the dust clouds move toward eastern China, extending to southern China at the same time on 18 March. After that, on 19 March, as shown in Figure 2a, the dust clouds moved further eastward and passed by Beijing and Tianjin, with the dust belt extended to southern China and Vietnam. However, the yellow dust did not reach the Korean peninsula, including the Korean east coast and Kangnung. Another dust belt was detected from Hokkaido in northern Japan to Honshu in the middle of Japan that extended to the east of the Philippines.

In Figure 2b, the METOP-B images show the dust belt from Vladivostok (Russia) to the Korean peninsula, including its east coast (Kangnung city, Republic of Korea), Kyusu Island (Japan), Taiwan and Luzon Island (Philippines) on 22 March, when PM_{10} concentration was very high at Kangnung during the yellow sand event from 00:01 LST, 21 March to 00:00 LST, 23 March. This dust belt is attributed to the transport of the previous dust belt that was on the line of Beijing–southern China–Vietnam on 19 March in Figure 2a.

3.2. Hourly PM_{10} , $PM_{2.5}$ and PM_1 Concentrations before, during and after the Dust Periods

Figures 3 and 4 indicate the hourly distribution of PM (PM_{10} and $PM_{2.5}$) and gas (SO_2 , CO, O_3 and NO_2) concentrations and meteorological parameters (air temperature, wind speed and relative humidity) at the Okcheonong observation point in Kangnung (Korea). Figure 5 also indicates the hourly distribution of PM (PM_{10} and $PM_{2.5}$) and gas (SO_2 , CO, O_3 and NO_2) concentrations at the Yongdingmen observation point in Beijing (China).

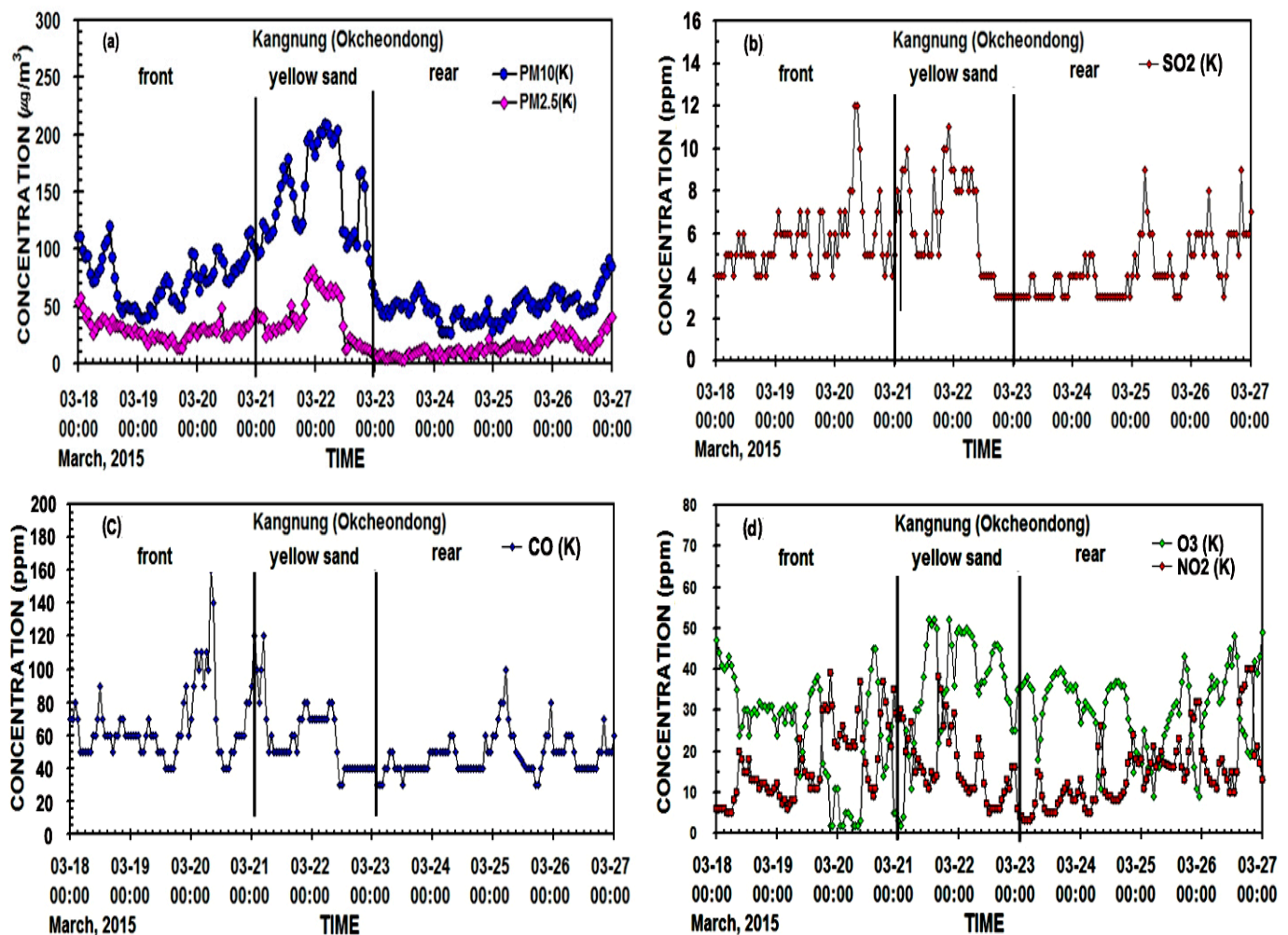


Figure 3. Hourly distribution of (a) PM₁₀ and PM_{2.5} concentrations ($\mu\text{g}/\text{m}^3$) and (b) SO₂ ($\times 1000$), (c) CO ($\times 100$), (d) O₃ ($\times 1000$) and NO₂ ($\times 1000$) concentrations (ppm) before, during and after the yellow sand period at the Okcheondong observation point in Kangnung city (Korea), corresponding to the PM concentrations on 16 to 25 March at the Yongdingmen observation point in Beijing city (China).

Choi and Zhang [17] indicated that the transportation of pollutants from Beijing (China) to Kangnung (Korea) takes about two days via a northwesterly wind of about 10 m/s. Thus, PM and gas pollutants for the second sand period in Beijing in Figure 5 may contribute to pollutant concentrations in Kangnung two days later in Figure 3. Thus, PM concentrations for the yellow sand event (on 00 LST, 21 March to 00 LST, 23 March) detected at the Okcheondong observation point in Kangnung could have been affected by PM and gaseous pollution at the Yongdingmen observation point in Beijing two days earlier (00 LST, 19 March to 00 LST, 21 March), corresponding to the second yellow sand period in Beijing.

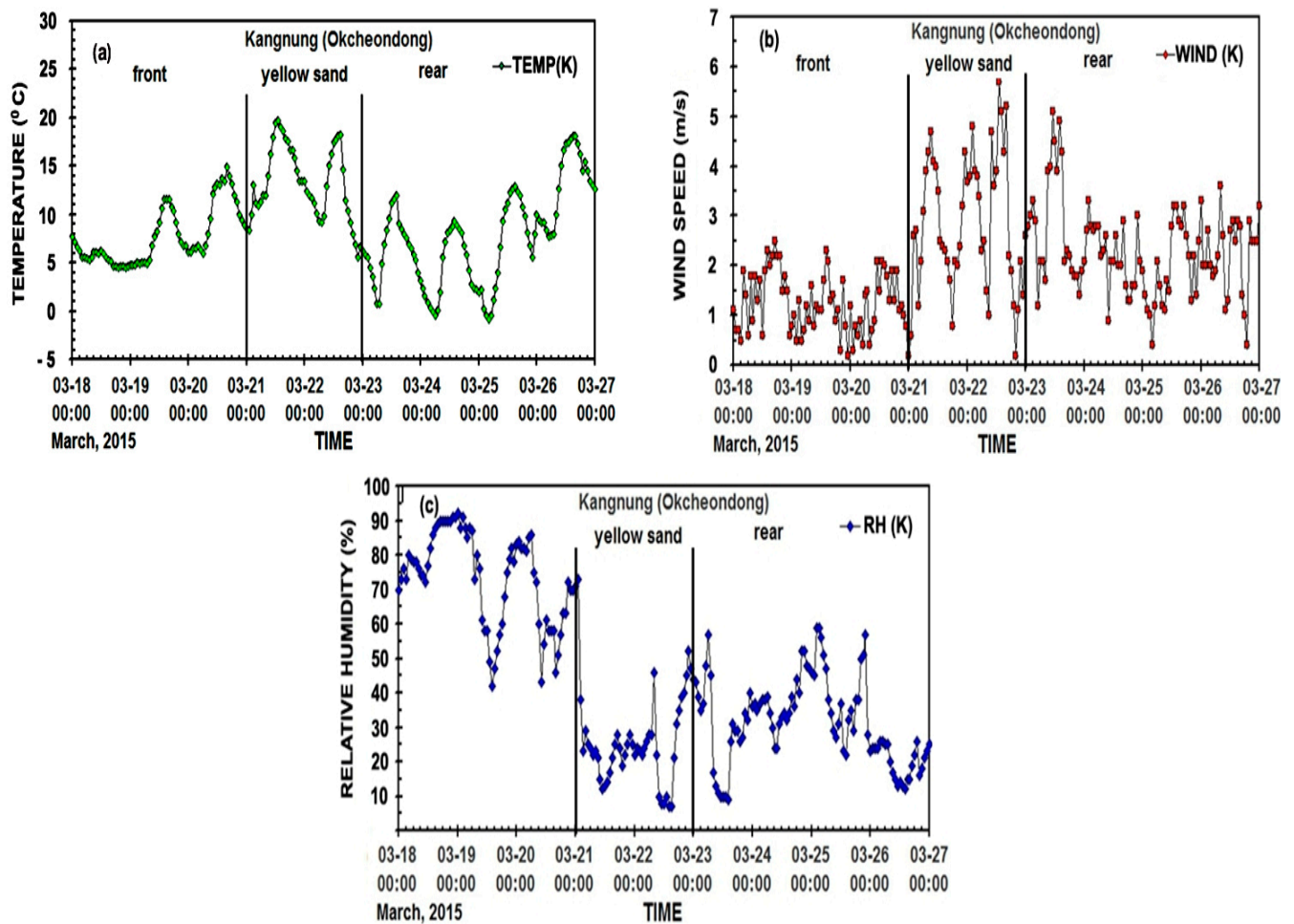


Figure 4. Hourly distributions of (a) air temperature ($^{\circ}\text{C}$; TEMP), (b) wind speed (m/s; WIND) and (c) relative humidity (%; RH) at Kangnung in Korea (modified from [41]).

In Figure 3, the PM_{10} concentration before the Yellow Sand event at Kangnung was about $50.445 \mu\text{g}/\text{m}^3$. When the PM_{10} concentration increased, the $\text{PM}_{2.5}$ concentration increased and had a mean value of $41.234 \mu\text{g}/\text{m}^3$. Both during the event (01:00 LST, 21 March to 00:00 LST, 23 March) and in the early stages after the event on 23 March, the PM_{10} and $\text{PM}_{2.5}$ concentrations rapidly increased; however, the increase in $\text{PM}_{2.5}$ was much smaller than that in PM_{10} . This may be attributed to the intrusion of major coarse particles of yellow sand into Kangnung. After the event, the temporal distributions of PM_{10} and $\text{PM}_{2.5}$ had a similar pattern, with similar magnitudes to those values of PM concentrations before the event with slightly different magnitudes.

We further investigated the effect of the ground-based concentrations of SO_2 , CO , O_3 and NO_2 at Kangnung in increasing the PM concentrations in Figure 3 before, during and after the yellow sand event from 00 LST, 18 March to 00 LST, 27 March. The SO_2 , NO_2 and CO concentrations had a similar temporal tendency to some extent, whereas O_3 had an opposite tendency. The concentrations before and during the event were slightly higher than ones after the event; however, the CO concentration relatively unchanged.

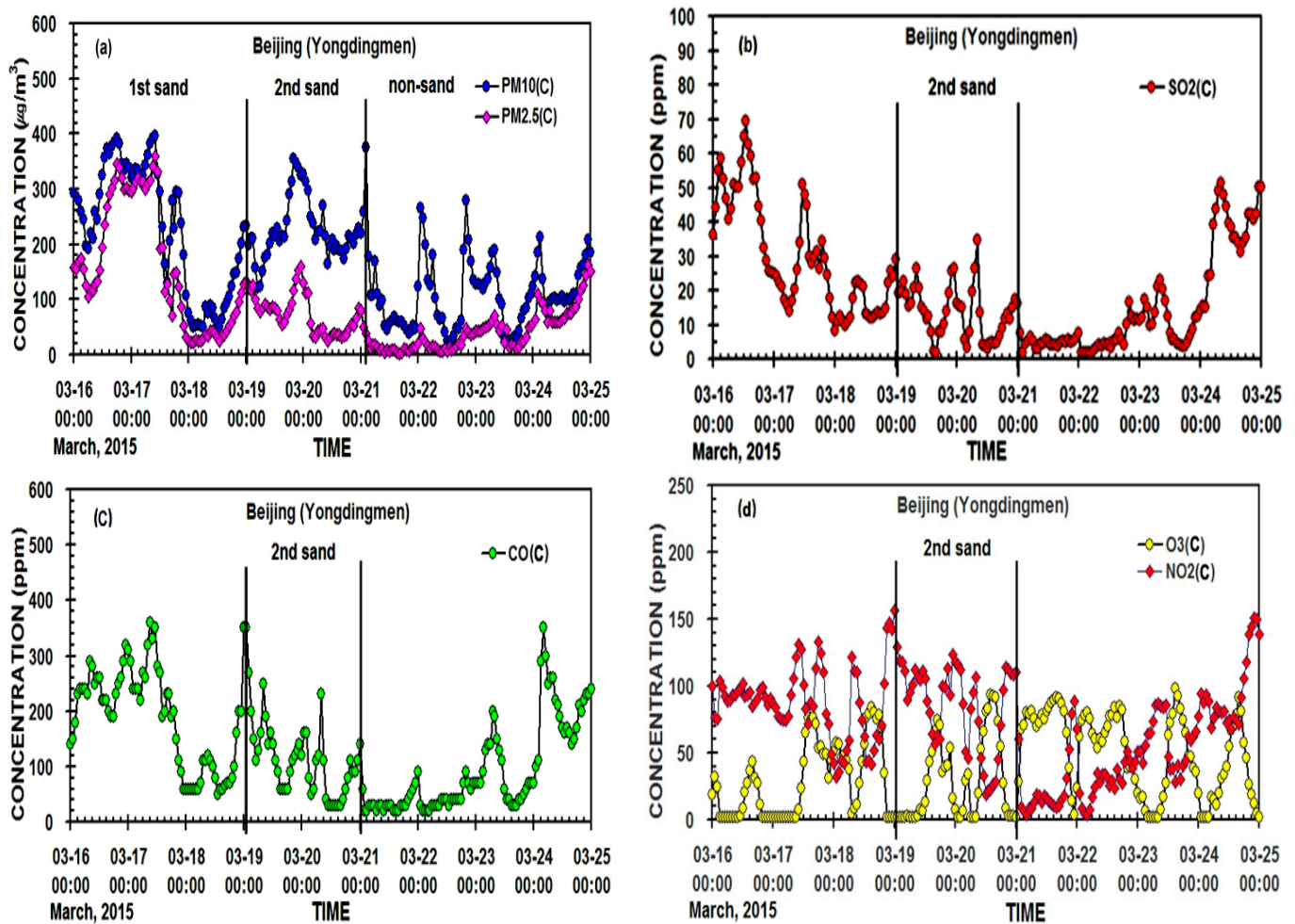


Figure 5. Hourly distribution of (a) PM_{10} and $PM_{2.5}$ concentrations ($\mu\text{g}/\text{m}^3$) and (b) SO_2 ($\times 1000$), (c) CO ($\times 100$), (d) O_3 ($\times 1000$) and NO_2 ($\times 1000$) concentrations (ppm) at the Yongdingmen observation point in Beijing (China), corresponding to PM concentrations on 18 to 27 March at Kangnung, Korea.

In Figure 3d shows, as Mendez et al [42] explained, that when the O_3 concentration increases, the NO_2 concentration decreases. A diurnal NO_x ($= NO_2 + O_3$) cycle shows that NO_x emitted from the vehicles on the road and heating boilers in residential areas undergoes its photochemical reaction into O_3 due to the increased daytime solar radiation, resulting in its decrease. In contrast, O_3 is reduced to NO_2 at night through the NO_x cycle (i.e., no photochemical reaction of NO_2), leading to a decrease in O_3 concentration. Chu et al. [43] insisted that the decreases in $PM_{2.5}$ and NO_2 concentrations support the control of NO_x to further reduce $PM_{2.5}$ pollution in China and result in the increase in O_3 concentrations.

We investigated whether meteorological parameters could influence PM and gas concentrations for the whole research period in Figure 4. The daytime air temperature near the ground surface during the yellow sand event at Kangnung (from 01:00 LST, 21 March to 00:00 LST 23 March) was much higher than in other periods. The maximum wind speed also became much higher than in other periods. The wind speed should be over 10 m/s (gust wind) for the dust mobilization in the desert. After the dust raised from the desert surface was uplifted to about a 3 km height, it was then transported a by westerly wind of 8 m/s to 10 m/s and moved to the downwind site of Kangnung 1400 km away. When high PM concentrations due to the dust were detected in Beijing, its local wind speed also

became higher, with a maximum of 5.8 m/s more than before; however, it was much lower due to the rough mountain topography surrounding the city than it was in the desert.

As the relative humidity had very low values of 6% to 54%, it was very dry without precipitation in Kangnung. During the yellow sand period at Kangnung, the hourly air temperature and wind speed increased more than in other periods but the relative humidity tended to decrease. Thus, these trends for the meteorological parameters may affect the PM and gas concentrations in the city in the presence of absence of yellow sand events.

Figure 5 shows that the SO₂ and CO concentrations during the second yellow sand period in Beijing from 00 LST, March 19 to 00 LST, March 21 decreased more markedly than before and after this period; however, as with the SO₂ and CO concentrations, the NO₂ concentration also slightly decreased but with smaller differences, whereas there was an opposite distribution of O₃ to NO₂ due to the NO_x cycle. Therefore, the gases in Beijing may affect the PM and gas concentrations at Kangnung.

3.3. Definition of Variables in the Multivariate Regression Model

A multivariate regression model consists of a set of independent variables as input data X_j to predict the dependent variable as output data Y_i, as shown in Table 1. This means that the 15 input variables include data for three hours earlier at Kangnung (PM (PM₁₀-K, PM_{2.5}-K), meteorological (TEMP_K, WIND_K, RH_K) and gas (SO₂-K, CO_K, O₃-K, NO₂-K)) and for 2 days earlier at Beijing (PM (PM₁₀-C, PM_{2.5}-C) and gas (SO₂-C, CO_C, O₃-C, NO₂-C)) that were used to make real-time output forecasting variables (PM₁₀-K(N), PM_{2.5}-K(N), SO₂-K(N), CO_K(N), O₃-K(N) and NO₂-K(N)) at Kangnung.

Table 1. Input and output variables in the multivariate regression model for real-time forecasting.

Input Variable		Output Variable
X ₁	PM ₁₀ -K: 3 h before	at Kangnung city, Korea Y ₁ PM ₁₀ -K(N): present (now) Y ₂ PM _{2.5} -K(N): present (now) Y ₃ SO ₂ -K(N): present (now) Y ₄ : CO_K(N): present (now) Y ₅ O ₃ -K(N): present (now) Y ₆ NO ₂ -K(N): present (now)
X ₂	PM _{2.5} -K: 3 h before	
X ₃	TEMP_K: 3 h before	
X ₄	WIND_K: 3 h before	
X ₅	RH_K: 3 h before	
X ₆	SO ₂ -K: 3 h before	
X ₇	CO_K: 3 h before	
X ₈	O ₃ -K: 3 h before	
X ₉	NO ₂ -K: 3 h before	
X ₁₀	PM ₁₀ -C: 2 days before	
X ₁₁	PM _{2.5} -C: 2 days before	
X ₁₂	SO ₂ -C: 2 days before	
X ₁₃	CO_C: 2 days before	
X ₁₄	O ₃ -C: 2 days before	
X ₁₅	NO ₂ -C: 2 days before	

3.4. Regression Equations and Correlation Matrix among PM₁₀, PM_{2.5}, SO₂, CO, O₃ and NO₂ Parameters (Kangnung) Affected by Meteorological Variables Associated with PM and Gases (Beijing)

A multiple regression equation consists of independent variables X_j to predict the dependent variable Y_i, such as in Equations (1) and (2).

$$\begin{aligned}
 Y_1 &= a_{11}X_1 + a_{12}X_2 + a_{13}X_3 + a_{14}X_4 + a_{15}X_5 + a_{16}X_6 + a_{17}X_7 + a_{18}X_8 + a_{19}X_9 \\
 &+ a_{110}X_{10} + a_{111}X_{11} + a_{112}X_{12} + a_{113}X_{13} + a_{114}X_{14} + a_{115}X_{15} + b_1 \\
 Y_2 &= a_{21}X_1 + a_{22}X_2 + a_{23}X_3 + a_{24}X_4 + a_{25}X_5 + a_{26}X_6 + a_{27}X_7 + a_{28}X_8 + a_{29}X_9 \\
 &+ a_{210}X_{10} + a_{211}X_{11} + a_{212}X_{12} + a_{213}X_{13} + a_{214}X_{14} + a_{215}X_{15} + b_2 \\
 Y_3 &= a_{31}X_1 + a_{32}X_2 + a_{33}X_3 + a_{34}X_4 + a_{35}X_5 + a_{36}X_6 + a_{37}X_7 + a_{38}X_8 + a_{39}X_9 \\
 &+ a_{310}X_{10} + a_{311}X_{11} + a_{312}X_{12} + a_{313}X_{13} + a_{314}X_{14} + a_{315}X_{15} + b_3 \\
 Y_4 &= a_{41}X_1 + a_{42}X_2 + a_{43}X_3 + a_{44}X_4 + a_{45}X_5 + a_{46}X_6 + a_{47}X_7 + a_{48}X_8 + a_{49}X_9 \\
 &+ a_{410}X_{10} + a_{411}X_{11} + a_{412}X_{12} + a_{413}X_{13} + a_{414}X_{14} + a_{415}X_{15} + b_1 \\
 Y_5 &= a_{51}X_1 + a_{52}X_2 + a_{53}X_3 + a_{54}X_4 + a_{55}X_5 + a_{56}X_6 + a_{57}X_7 + a_{58}X_8 + a_{59}X_9 \\
 &+ a_{510}X_{10} + a_{511}X_{11} + a_{512}X_{12} + a_{513}X_{13} + a_{514}X_{14} + a_{515}X_{15} + b_2 \\
 Y_6 &= a_{61}X_1 + a_{62}X_2 + a_{63}X_3 + a_{64}X_4 + a_{65}X_5 + a_{66}X_6 + a_{67}X_7 + a_{68}X_8 + a_{69}X_9 \\
 &+ a_{610}X_{10} + a_{611}X_{11} + a_{612}X_{12} + a_{613}X_{13} + a_{614}X_{14} + a_{615}X_{15} + b_3
 \end{aligned}
 \tag{1}$$

Equation (1) can be rewritten in a matrix form as below.

$$\begin{bmatrix} Y_1 \\ Y_2 \\ Y_3 \\ Y_4 \\ Y_5 \\ Y_6 \end{bmatrix} = \begin{bmatrix} a_{11} & a_{12} & \dots & a_{115} \\ a_{21} & a_{22} & \dots & a_{215} \\ a_{31} & a_{32} & \dots & a_{315} \\ a_{41} & a_{42} & \dots & a_{415} \\ a_{51} & a_{52} & \dots & a_{515} \\ a_{61} & a_{62} & \dots & a_{615} \end{bmatrix} \begin{bmatrix} X_1 \\ X_2 \\ X_3 \\ X_4 \\ X_5 \\ X_6 \\ X_7 \\ X_8 \\ X_9 \\ X_{10} \\ X_{11} \\ X_{12} \\ X_{13} \\ X_{14} \\ X_{15} \end{bmatrix} + \begin{bmatrix} b_1 \\ b_2 \\ b_3 \\ b_4 \\ b_5 \\ b_6 \end{bmatrix}
 \tag{2}$$

where a_{ij} ($i = 1$ to 6 ; $j = 1$ to 15) indicates the coefficient of the matrix and the measured values of X_j (j ; represents the number of independent variables; $j = 1$ to 15) such as PM_{10_K} , $PM_{2.5_K}$, $TEMP_K$ (air temperature), $WIND_K$ (wind speed), RH_K (relative humidity), SO_2_K , CO_K , O_3_K , NO_2_K , PM_{10_C} , $PM_{2.5_C}$, SO_2_C , CO_C , O_3_C and NO_2_C . The real-time predictive values Y_i ($i = 1$ to 6 ; $PM_{10_K(N)}$, $PM_{2.5_K(N)}$, $SO_2_K(N)$, $CO_K(N)$, $O_3_K(N)$ and $NO_2_K(N)$) are dependent variables and b_i ($i = 1$ to 6) is an error term that intercepts in the equations of Y_i .

In this study, our prediction models comprise multiple predictive regression equations on each PM_{10_K} , $PM_{2.5_K}$, SO_2_K , CO_K , O_3_K and NO_2_K value that are influenced by not only meteorological and gas parameters of the city but also PM_{10_C} , $PM_{2.5_C}$, SO_2_C , CO_C , O_3_C and NO_2_C concentrations. Tables 2–4 shows multiple correlation coefficients and predictive regression equations on each PM and gas concentration at Kangnung before, during and after the yellow sand periods in three classifications through multiple regression analyses using SPSS statistics software v27.

Table 2. Multivariate correlation coefficients and predictive regression equations for real-time PM_{10_K(N)}, PM_{2.5_K(N)}, SO_{2_K(N)}, CO_{K(N)}, O_{3_K(N)} and NO_{2_K(N)} values at Kangnung, Korea (K) affected by meteorological parameters associated with the PM and gases in Beijing, China (C) before the Yellow Sand event, 2015.

Period	Multi-Correlation Coefficient (r)		Multivariate Predictive Regression Equation
18–21 March 2015 Before the Yellow Sand Event	0.957	PM10_K(N)	= 0.559 × PM _{10_K} − 0.175 × PM _{2.5_K} + 2.362 × TEMP_K − 1.355 × WIND_K − 0.477 × RH_K − 2.982 × SO _{2_K} + 0.162 × CO_K − 0.143 × O _{3_K} + 0.304 × NO _{2_K} + 0.036 × PM _{10_C} − 0.036 × PM _{2.5_C} + 0.340 × SO _{2_C} − 0.064 × CO_C − 0.500 × O _{3_C} − 0.148 × NO _{2_C} + 87.948
	0.906	PM _{2.5_K(N)}	= 0.122 × PM _{10_K} + 0.452 × PM _{2.5_K} − 0.164 × TEMP_K + 0.291 × WIND_K + 0.204 × RH_K − 0.257 × SO _{2_K} + 0.148 × CO_K + 0.526 × O _{3_K} + 0.565 × NO _{2_K} + 0.002 × PM _{10_C} − 0.008 × PM _{2.5_C} − 0.075 × SO _{2_C} + 0.013 × CO_C + 0.005 × O _{3_C} + 0.006 × NO _{2_C} − 37.838
	0.886	NO _{2_K(N)}	= 0.001 × PM _{10_K} − 0.058 × PM _{2.5_K} − 0.332 × TEMP_K − 1.788 × WIND_K + 0.194 × RH_K + 0.407 × SO _{2_K} − 0.016 × CO_K + 0.156 × O _{3_K} + 0.784 × NO _{2_K} + 0.001 × PM _{10_C} − 0.019 × PM _{2.5_C} − 0.070 × SO _{2_C} − 0.006 × CO_C + 0.124 × O _{3_C} + 0.153 × NO _{2_C} − 19.762
	0.795	SO _{2_K(N)}	= −0.013 × PM _{10_K} − 0.012 × PM _{2.5_K} + 0.196 × TEMP_K − 0.415 × WIND_K + 0.030 × RH_K + 0.521 × SO _{2_K} + 0.009 × CO_K − 0.040 × O _{3_K} − 0.065 × NO _{2_K} − 0.007 × PM _{10_C} + 0.003 × PM _{2.5_C} + 0.021 × SO _{2_C} − 0.001 × CO_C − 0.001 × O _{3_C} + 0.016 × NO _{2_C} + 1.682
	0.932	O _{3_K(N)}	= −0.033 × PM _{10_K} + 0.012 × PM _{2.5_K} + 1.353 × TEMP_K + 2.838 × WIND_K − 0.218 × RH_K + 0.111 × SO _{2_K} + 0.043 × CO_K + 0.564 × O _{3_K} − 0.221 × NO _{2_K} + 0.001 × PM _{10_C} + 0.022 × PM _{2.5_C} + 0.183 × SO _{2_C} + 0.001 × CO_C − 0.172 × O _{3_C} − 0.182 × NO _{2_C} + 26.519
	0.864	CO_K(N)	= −0.033 × PM _{10_K} + 0.423 × PM _{2.5_K} + 0.141 × TEMP_K + 1.200 × WIND_K + 0.235 × RH_K − 0.412 × SO _{2_K} + 0.372 × CO_K − 1.404 × O _{3_K} − 1.510 × NO _{2_K} + 0.073 × PM _{10_C} − 0.096 × PM _{2.5_C} − 0.056 × SO _{2_C} − 0.068 × CO_C + 0.025 × O _{3_C} + 0.221 × NO _{2_C} + 67.539

Table 3. As shown in Table 2, except during the yellow sand event.

Period	Multi-Correlation Coefficient (r)		Multivariate Predictive Regression Equation
21–23 March 2015 During the Yellow Sand Event	0.936	PM ₁₀ _K(N)	= 0.656 × PM ₁₀ _K − 0.339 × PM _{2.5} _K − 2.780 × TEMP_K + 3.634 × WIND_K − 0.658 × RH_K − 0.661 × SO ₂ _K + 0.698 × CO_K + 1.616 × O ₃ _K + 1.288 × NO ₂ _K + 0.122 × PM ₁₀ _C − 0.289 × PM _{2.5} _C − 0.332 × SO ₂ _C + 0.168 × CO_C + 0.324 × O ₃ _C + 0.367 × NO ₂ _C − 73.497
	0.982	PM _{2.5} _K(N)	= 0.102 × PM ₁₀ _K + 0.261 × PM _{2.5} _K − 0.570 × TEMP_K + 0.362 × WIND_K + 0.043 × RH_K + 0.651 × SO ₂ _K + 0.263 × CO_K + 0.860 × O ₃ _K + 0.699 × NO ₂ _K + 0.055 × PM ₁₀ _C + 0.049 × PM _{2.5} _C + 0.025 × SO ₂ _C + 0.079 × CO_C − 0.007 × O ₃ _C − 0.150 × NO ₂ _C − 56.162
	0.866	NO ₂ _K(N)	= − 0.043 × PM ₁₀ _K + 0.062 × PM _{2.5} _K + 0.617 × TEMP_K − 1.998 × WIND_K + 0.081 × RH_K + 0.114 × SO ₂ _K + 0.030 × CO_K + 0.300 × O ₃ _K + 0.736 × NO ₂ _K − 0.039 × PM ₁₀ _C − 0.039 × PM _{2.5} _C + 0.176 × SO ₂ _C + 0.020 × CO_C + 0.069 × O ₃ _C + 0.070 × NO ₂ _C − 11.366
	0.917	SO ₂ _K(N)	= − 0.010 × PM ₁₀ _K + 0.013 × PM _{2.5} _K − 0.067 × TEMP_K − 0.326 × WIND_K − 0.035 × RH_K + 0.041 × SO ₂ _K + 0.063 × CO_K + 0.116 × O ₃ _K + 0.097 × NO ₂ _K + 0.003 × PM ₁₀ _C + 0.024 × PM _{2.5} _C + 0.022 × SO ₂ _C + 0.007 × CO_C − 0.038 × O ₃ _C − 0.058 × NO ₂ _C + 2.650
	0.916	O ₃ _K(N)	= 0.036 × PM ₁₀ _K − 0.118 × PM _{2.5} _K + 0.326 × TEMP_K + 2.790 × WIND_K − 0.127 × RH_K − 0.819 × SO ₂ _K + 0.046 × CO_K + 0.395 × O ₃ _K + 0.132 × NO ₂ _K + 0.106 × PM ₁₀ _C − 0.009 × PM _{2.5} _C − 0.010 × SO ₂ _C − 0.025 × CO_C − 0.211 × O ₃ _C − 0.132 × NO ₂ _C + 10.742
	0.887	CO_K(N)	= − 0.096 × PM ₁₀ _K + 0.071 × PM _{2.5} _K + 1.654 × TEMP_K − 3.874 × WIND_K + 0.365 × RH_K + 3.152 × SO ₂ _K + 0.460 × CO_K + 0.216 × O ₃ _K − 0.570 × NO ₂ _K + 0.008 × PM ₁₀ _C + 0.050 × PM _{2.5} _C − 0.015 × SO ₂ _C + 0.099 × CO_C − 0.166 × O ₃ _C − 0.191 × NO ₂ _C + 9.089

Multiple correlation coefficients among the real-time predicted PM₁₀_K, PM_{2.5}_K, SO₂_K, CO_K, O₃_K and NO₂_K values were in the range of 0.795 to 0.982. In particular, the correlation coefficients for PM₁₀_K, PM_{2.5}_K, NO₂_K, SO₂_K, O₃_K and CO_K before (during; after) the yellow sand periods were 0.957 (0.936; 0.919), 0.906 (0.982; 0.945), 0.886 (0.866; 0.902), 0.795 (0.917; 0.857), 0.932 (0.916; 0.892) and 0.864 (0.887; 0.887), respectively.

Correlation analysis of PM₁₀_K, PM_{2.5}_K, SO₂_K, CO_K, O₃_K and NO₂_K shows that the values were significantly correlated at $p < 0.001$, though their partial correlation coefficients were different in Tables 5 and 6. In particular, as the correlation coefficients between the predicted and measured values of PM₁₀ (PM_{2.5}) for the whole period were very high, 0.919 to 0.957 (0.906 to 0.982), the values predicted by the model were very close to the measured values, reflecting the measured values quite well.

Table 4. As shown in Table 2, except for after the yellow sand event.

Period	Multi-Correlation Coefficient (r)		Multivariate Predictive Regression Equation
23–27 March 2015 After the Yellow Sand event	0.919	PM ₁₀ _K(N)	= 0.866 × PM ₁₀ _K – 0.242 × PM _{2.5} _K – 0.529 × TEMP_K + 1.037 × WIND_K – 0.056 × RH_K – 0.838 × SO ₂ _K + 0.059 × CO_K + 0.088 × O ₃ _K + 0.373 × NO ₂ _K – 0.012 × PM ₁₀ _C + 0.038 × PM _{2.5} _C – 0.001 × SO ₂ _C + 0.006 × CO_C + 0.047 × O ₃ _C + 0.086 × NO ₂ _C – 1.486
	0.945	PM _{2.5} _K(N)	= 0.060 × PM ₁₀ _K + 0.575 × PM _{2.5} _K – 0.235 × TEMP_K + 0.630 × WIND_K + 0.024 × RH_K – 0.368 × SO ₂ _K + 0.095 × CO_K + 0.316 × O ₃ _K + 0.413 × NO ₂ _K – 0.008 × PM ₁₀ _C + 0.064 × PM _{2.5} _C – 0.033 × SO ₂ _C + 0.003 × CO_C – 0.033 × O ₃ _C – 0.027 × NO ₂ _C – 13.986
	0.902	NO ₂ _K(N)	= – 0.117 × PM ₁₀ _K + 0.084 × PM _{2.5} _K – 0.119 × TEMP_K – 0.178 × WIND_K + 0.136 × RH_K – 1.015 × SO ₂ _K – 0.064 × CO_K – 0.045 × O ₃ _K + 0.761 × NO ₂ _K – 0.006 × PM ₁₀ _C – 0.010 × PM _{2.5} _C + 0.016 × SO ₂ _C + 0.024 × CO_C + 0.110 × O ₃ _C + 0.101 × NO ₂ _C + 1.605
	0.857	SO ₂ _K(N)	= 0.002 × PM ₁₀ _K – 0.033 × PM _{2.5} _K – 0.121 × TEMP_K – 0.038 × WIND_K – 0.002 × RH_K + 0.112 × SO ₂ _K + 0.038 × CO_K + 0.032 × O ₃ _K + 0.044 × NO ₂ _K – 0.005 × PM ₁₀ _C + 0.030 × PM _{2.5} _C – 0.005 × SO ₂ _C + 0.005 × CO_C + 0.009 × O ₃ _C + 0.001 × NO ₂ _C + 0.372
	0.892	O ₃ _K(N)	= 0.120 × PM ₁₀ _K + 0.021 × PM _{2.5} _K + 0.507 × TEMP_K + 0.296 × WIND_K – 0.165 × RH_K + 1.445 × SO ₂ _K + 0.056 × CO_K + 0.642 × O ₃ _K – 0.187 × NO ₂ _K + 0.007 × PM ₁₀ _C – 0.014 × PM _{2.5} _C – 0.016 × SO ₂ _C – 0.022 × CO_C – 0.065 × O ₃ _C – 0.053 × NO ₂ _C + 7.410
	0.887	CO_K(N)	= – 0.085 × PM ₁₀ _K – 0.444 × PM _{2.5} _K – 1.192 × TEMP_K – 0.386 × WIND_K + 0.126 × RH_K – 2.236 × SO ₂ _K + 0.512 × CO_K + 0.451 × O ₃ _K + 0.737 × NO ₂ _K – 0.072 × PM ₁₀ _C + 0.291 × PM _{2.5} _C + 0.019 × SO ₂ _C + 0.014 × CO_C – 0.146 × O ₃ _C – 0.160 × NO ₂ _C + 34.936

Table 5. Partial correlation coefficient matrix of variables to PM₁₀-K(N) in a multivariate regression model for Kangnung before the yellow sand event, 2015.

Pearson Correlation Coefficient (r) before the Yellow Sand Event																
Item	PM ₁₀ -K(N)	PM ₁₀ -K	PM _{2.5} -K	TEMP_K	WIND_K	RH_K	SO ₂ -K	CO_K	O ₃ -K	NO ₂ -K	PM ₁₀ -C	PM _{2.5} -C	SO ₂ -C	CO_C	O ₃ -C	NO ₂ -C
PM ₁₀ -K(N)	1.000	0.910	0.591	0.306	-0.164	-0.306	0.103	0.360	-0.175	0.418	-0.356	-0.527	0.217	-0.322	-0.004	0.158
PM ₁₀ -K		1.000	0.671	0.279	-0.099	-0.270	0.083	0.330	-0.112	0.331	-0.339	-0.489	0.271	-0.321	0.052	0.078
PM _{2.5} -K			1.000	-0.122	-0.054	0.114	-0.117	0.246	0.162	-0.087	-0.016	-0.086	0.383	-0.072	-0.298	0.028
TEMP_K				1.000	0.192	-0.896	0.167	-0.239	0.081	0.338	-0.556	-0.600	-0.345	-0.512	0.742	-0.103
WIND_K					1.000	-0.152	-0.238	-0.424	0.359	-0.178	0.136	0.148	0.188	0.039	0.220	0.034
RH_K						1.000	-0.197	0.255	-0.162	-0.226	0.434	0.514	0.105	0.278	-0.655	-0.030
SO ₂ -K							1.000	0.590	-0.531	0.483	-0.373	-0.268	-0.303	-0.280	0.069	-0.062
CO_K								1.000	-0.690	0.475	-0.313	-0.263	-0.137	-0.279	-0.227	-0.002
O ₃ -K									1.000	-0.822	0.376	0.318	0.416	0.329	0.010	-0.006
NO ₂ -K										1.000	-0.418	-0.473	-0.348	-0.448	0.233	0.086
PM ₁₀ -C											1.000	0.925	0.584	0.805	-0.535	0.486
PM _{2.5} -C												1.000	0.410	0.775	-0.540	0.352
SO ₂ -C													1.000	0.549	-0.330	0.412
CO_C														1.000	-0.634	0.617
O ₃ -C															1.000	-0.529
NO ₂ -C																1.000

Pearson Correlation Coefficient (r) before the Yellow Sand event																
Item	PM _{2.5} -K(N)	PM ₁₀ -K	PM _{2.5} -K	TEMP_K	WIND_K	RH_K	SO ₂ -K	CO_K	O ₃ -K	NO ₂ -K	PM ₁₀ -C	PM _{2.5} -C	SO ₂ -C	CO_C	O ₃ -C	NO ₂ -C
PM _{2.5} -K(N)	1.000	0.701	0.826	-0.105	-0.090	0.148	-0.047	0.375	0.035	0.086	-0.030	-0.136	0.314	-0.108	-0.301	0.091

Pearson Correlation Coefficient (r) before the Yellow Sand event																
Item	SO ₂ -K(N)	PM ₁₀ -K	PM _{2.5} -K	TEMP_K	WIND_K	RH_K	SO ₂ -K	CO_K	O ₃ -K	NO ₂ -K	PM ₁₀ -C	PM _{2.5} -C	SO ₂ -C	CO_C	O ₃ -C	NO ₂ -C
NO ₂ -K(N)	1.000	0.244	-0.179	0.367	-0.196	-0.252	0.379	0.360	-0.677	0.842	-0.397	-0.475	-0.357	-0.409	0.258	0.153

Pearson Correlation Coefficient (r) before the Yellow Sand event																
Item	SO ₂ -K(N)	PM ₁₀ -K	PM _{2.5} -K	TEMP_K	WIND_K	RH_K	SO ₂ -K	CO_K	O ₃ -K	NO ₂ -K	PM ₁₀ -C	PM _{2.5} -C	SO ₂ -C	CO_C	O ₃ -C	NO ₂ -C
SO ₂ -K(N)	1.000	0.004	-0.149	0.049	-0.328	-0.049	0.704	0.557	-0.513	0.351	-0.364	-0.251	-0.302	-0.210	-0.030	0.025

Table 5. Cont.

Pearson Correlation Coefficient (r) before the Yellow Sand event																
Item	O ₃ _K(N)	PM ₁₀ _K	PM _{2.5} _K	TEMP_K	WIND_K	RH_K	SO ₂ _K	CO_K	O ₃ _K	NO ₂ _K	PM ₁₀ _C	PM _{2.5} _C	SO ₂ _C	CO_C	O ₃ _C	NO ₂ _C
O ₃ _K(N)	1.000	-0.084	0.190	0.070	0.396	-0.172	-0.378	-0.578	0.899	-0.748	0.333	0.319	0.425	0.301	0.011	-0.070
Pearson Correlation Coefficient (r) before the Yellow Sand event																
Item	CO_K(N)	PM ₁₀ _K	PM _{2.5} _K	TEMP_K	WIND_K	RH_K	SO ₂ _K	CO_K	O ₃ _K	NO ₂ _K	PM ₁₀ _C	PM _{2.5} _C	SO ₂ _C	CO_C	O ₃ _C	NO ₂ _C
CO_K(N)	1.000	0.264	0.209	-0.267	-0.355	0.326	0.344	0.769	-0.670	0.418	-0.301	-0.285	-0.175	-0.287	-0.226	0.033

Table 6. Partial correlation coefficient matrix of variables to PM₁₀-K(N) in a multivariate regression model for Kangnung during the yellow sand event, 2015.

Pearson Correlation Coefficient (r) during the Yellow Sand Event																
Item	PM ₁₀ _K(N)	PM ₁₀ _K	PM _{2.5} _K	TEMP_K	WIND_K	RH_K	SO ₂ _K	CO_K	O ₃ _K	NO ₂ _K	PM ₁₀ _C	PM _{2.5} _C	SO ₂ _C	CO_C	O ₃ _C	NO ₂ _C
PM ₁₀ _K(N)	1.000	0.884	0.749	0.087	0.209	-0.240	0.544	0.215	0.564	-0.015	0.460	0.063	0.181	0.003	-0.176	0.116
PM ₁₀ _K		1.000	0.769	0.048	0.157	-0.226	0.485	0.143	0.576	-0.083	0.351	-0.077	0.065	-0.110	-0.159	0.028
PM _{2.5} _K			1.000	0.032	0.115	-0.054	0.759	0.499	0.301	0.271	0.526	0.297	0.237	0.161	-0.187	0.139
TEMP_K				1.000	0.430	-0.767	-0.027	-0.311	0.472	-0.050	0.166	-0.051	-0.518	-0.454	0.699	-0.507
WIND_K					1.000	-0.690	-0.014	-0.293	0.498	-0.494	-0.044	-0.197	-0.220	-0.286	0.307	-0.409
RH_K						1.000	-0.014	0.404	-0.641	0.387	-0.007	0.288	0.407	0.592	-0.542	0.565
SO ₂ _K							1.000	0.777	-0.034	0.554	0.321	0.437	0.436	0.258	-0.274	0.235
CO_K								1.000	-0.496	0.651	0.040	0.471	0.490	0.551	-0.471	0.410
O ₃ _K									1.000	-0.604	0.337	-0.290	-0.348	-0.542	0.351	-0.366
NO ₂ _K										1.000	0.326	0.619	0.382	0.420	-0.218	0.423
PM ₁₀ _C											1.000	0.547	0.217	0.058	-0.002	0.286
PM _{2.5} _C												1.000	0.584	0.608	-0.420	0.719
SO ₂ _C													1.000	0.766	-0.686	0.750
CO_C														1.000	-0.711	0.779
O ₃ _C															1.000	-0.867

Table 6. Cont.

Pearson Correlation Coefficient (r) during the Yellow Sand event																
Item	PM _{2.5} _K(N)	PM ₁₀ _K	PM _{2.5} _K	TEMP_K	WIND_K	RH_K	SO ₂ _K	CO_K	O ₃ _K	NO ₂ _K	PM ₁₀ _C	PM _{2.5} _C	SO ₂ _C	CO_C	O ₃ _C	NO ₂ _C
PM _{2.5} _K(N)	1.000	0.748	0.932	0.066	0.065	−0.044	0.797	0.522	0.331	0.332	0.624	0.399	0.328	0.213	−0.208	0.229
Pearson Correlation Coefficient (r) during the Yellow Sand event																
Item	NO ₂ _K(N)	PM ₁₀ _K	PM _{2.5} _K	TEMP_K	WIND_K	RH_K	SO ₂ _K	CO_K	O ₃ _K	NO ₂ _K	PM ₁₀ _C	PM _{2.5} _C	SO ₂ _C	CO_C	O ₃ _C	NO ₂ _C
NO ₂ _K(N)	1.000	−0.033	0.235	0.044	−0.539	0.327	0.446	0.526	−0.389	0.778	0.256	0.490	0.330	0.393	−0.146	0.361
Pearson Correlation Coefficient (r) during the Yellow Sand event																
Item	SO ₂ _K(N)	PM ₁₀ _K	PM _{2.5} _K	TEMP_K	WIND_K	RH_K	SO ₂ _K	CO_K	O ₃ _K	NO ₂ _K	PM ₁₀ _C	PM _{2.5} _C	SO ₂ _C	CO_C	O ₃ _C	NO ₂ _C
SO ₂ _K(N)	1.000	0.398	0.723	0.002	−0.091	0.050	0.847	0.741	−0.012	0.520	0.414	0.523	0.410	0.332	−0.281	0.291
Pearson Correlation Coefficient (r) during the Yellow Sand event																
Item	O ₃ _K(N)	PM ₁₀ _K	PM _{2.5} _K	TEMP_K	WIND_K	RH_K	SO ₂ _K	CO_K	O ₃ _K	NO ₂ _K	PM ₁₀ _C	PM _{2.5} _C	SO ₂ _C	CO_C	O ₃ _C	NO ₂ _C
O ₃ _K(N)	1.000	0.480	0.279	0.476	0.607	−0.665	0.004	−0.428	0.829	−0.437	0.420	−0.157	−0.286	−0.483	0.285	−0.292
Pearson Correlation Coefficient (r) during the Yellow Sand event																
Item	CO_K(N)	PM ₁₀ _K	PM _{2.5} _K	TEMP_K	WIND_K	RH_K	SO ₂ _K	CO_K	O ₃ _K	NO ₂ _K	PM ₁₀ _C	PM _{2.5} _C	SO ₂ _C	CO_C	O ₃ _C	NO ₂ _C
CO_K(N)	1.000	0.124	0.471	−0.251	−0.343	0.417	0.667	0.826	−0.365	0.555	0.141	0.517	0.497	0.607	−0.457	0.458

In Table 5, a partial correlation coefficients matrix before the yellow sand period, predicted that the current PM_{10_K(N)} in Kangnung is positively influenced by not only the PM_{10_K} (0.910; highest), PM_{2.5_K} (0.591; 2nd high), NO_{2_K}, CO_K, TEMP_K and SO_{2_K} in Kangnung, which had relatively high contributions, but also both SO_{2_C} and NO_{2_C} in Beijing, which had a little contribution. A variable with a minus sign implies negatively contributing to the PM_{10_K(N)} concentration. PM_{2.5_C}, PM_{10_C}, CO_C and O_{3_C} contributed to the predicted PM_{10_K(N)} negatively. The predicted PM_{2.5_K(N)} is positively influenced by the measured PM_{2.5_K} (0.826; highest), PM_{10_K} (0.701; 2nd high), CO_K, RH_K, NO_{2_K} and O_{3_K} in Kangnung. However, it is a little influenced by the SO_{2_C} and NO_{2_C} values in Beijing city. The others negatively influenced it.

The predicted NO_{2_K(N)} is highly positively influenced by the measured NO_{2_K} (0.842; highest), SO_{2_K} (0.379; 2nd high), TEMP_K, CO_K and PM_{10_K} in Kangnung but is a little influenced by the O_{3_C} and NO_{2_C} in Beijing; the other variables negatively influence the predicted NO_{2_K(N)}. The predicted SO_{2_K(N)} is positively influenced by the measured SO_{2_K} (0.704; highest), CO_K (0.557; 2nd high), NO_{2_K}, TEMP_K and PM_{10_K} in Kangnung and the NO_{2_C} in Beijing. The other variables affect it negatively. The predicted O_{3_K(N)} is positively influenced by the measured O_{3_K} (0.899; highest), WIND_K, PM_{2.5_K} and TEMP_K in Kangnung and SO_{2_C} (0.425; 2nd high), PM_{10_C}, PM_{2.5_C}, CO_C and O_{3_C} in Beijing; the other variables have a negative influence. Only O_{3_K(N)} is more positively influenced by the PM and gas in Beijing.

The predicted CO_K(N) is positively influenced by the measured CO_K (0.769; highest), NO_{2_K} (0.418; 2nd high), SO_{2_K}, RH_K, PM_{10_K} and PM_{2.5_K} in Kangnung but is a little influenced by the NO_{2_C} in Beijing; the other variables have a negative influence. Among the six real-time predicted variables, five (except for O_{3_K(N)}) in Kangnung were negatively influenced by all of the PM in Beijing; however, they were negatively or positively influenced by the gases in Beijing.

In Table 6, during the yellow sand event, the predicted PM_{10_K(N)} is highly positively influenced by the measured PM_{10_K} (0.884; highest), PM_{2.5_K} (0.749; second highest), O_{3_K}, SO_{2_K}, CO_K, WIND_K and TEMP_K in Kangnung but is a little influenced by the PM_{10_C}, SO_{2_C}, NO_{2_C}, PM_{2.5_C} and CO_C in Beijing. The other variables had a negative influence on it. Thus, all of the PM and gas values in Beijing influenced it, except for O_{3_C}. The predicted PM_{2.5_K(N)} is highly positively influenced by the measured PM_{2.5_K} (0.932; highest), SO_{2_K} (0.797; second highest), PM_{10_K}, CO_K, O_{3_K}, NO_{2_K}, TEMP_K and WIND_K in Kangnung but is significantly influenced by the PM_{10_C}, PM_{2.5_C}, SO_{2_C}, CO_C and NO_{2_C} in Beijing. In contrast, O_{3_C} and RH_K affected it negatively. All of the PM and gas values in Beijing influenced it, except for O_{3_C}.

The predicted O_{3_K(N)} is positively influenced by the measured O_{3_K} (0.829; highest), WIND_K (0.607; second highest), PM_{10_K}, TEMP_K, PM_{2.5_K} and SO_{2_K} in Kangnung and the PM_{10_C}, O_{3_C} in Beijing; the other variables affected it negatively. The predicted CO_K(N) is positively affected by the measured CO_K (0.826; highest), SO_{2_K} (0.667; second highest), NO_{2_K}, PM_{2.5_K}, RH_K and PM_{10_K} in Kangnung and the CO_C, PM_{2.5_C}, SO_{2_C}, NO_{2_C} and PM_{10_C} in Beijing. However, O_{3_C}, O_{3_K}, WIND_K and TEMP_K affect it negatively. Five real-time predicted variables (except for O_{3_K(N)}) in Kangnung are most positively influenced by all of the PM and gas (except for O_{3_C}) values in Beijing. Therefore, the PM and gas (except for O_{3_C}) values in Beijing highly affected the predicted PM and gas values in Kangnung.

In Table 7, after the yellow sand event, the predicted PM_{10_K(N)} is positively influenced by the measured PM_{10_K} (0.888; highest), PM_{2.5_K} (0.606; second highest), TEMP_K, NO_{2_K}, SO_{2_K}, O_{3_K}, WIND_K and CO_K in Kangnung and the NO_{2_C}, PM_{2.5_C}, SO_{2_C}, CO_C and PM_{10_C} in Beijing, with a high effect on the predicted PM_{10_K(N)}. The other variables affected it negatively. The predicted PM_{2.5_K(N)} is positively influenced by the measured PM_{2.5_K} (0.921; highest), SO_{2_K}, PM_{10_K}, NO_{2_K}, TEMP_K and CO_K in Kangnung and the PM_{2.5_C} (0.819; second highest), NO_{2_C}, CO_C, SO_{2_C} and PM_{10_C} in Beijing. Beijing's measured PM and gas greatly contributed to the increase in the predicted

PM_{2.5}_K(N). The other variables affected it negatively. Thus, the PM and gas in Beijing (except for O₃_C) greatly contributed to the increase in both PM₁₀_K(N) and PM_{2.5}_K(N).

The predicted NO₂_K(N) is positively influenced by the measured NO₂_K (0.855; highest), PM_{2.5}_K, SO₂_K, TEMP_K, CO_K, PM₁₀_K and RH_K in Kangnung and the NO₂_C (0.564; second highest), PM_{2.5}_C, SO₂_C, CO_C and PM₁₀_C in Beijing; O₃_K, WIND_K and O₃_C affect it negatively. The measured PM and gas (except for O₃_C) in Beijing greatly contributed to the increase in the predicted NO₂_K(N). O₃_K contributes negatively to it through NO_x cycle processes. The predicted SO₂_K(N) is positively influenced by the measured SO₂_K (0.751; highest), CO_K, PM_{2.5}_K, NO₂_K, PM₁₀_K, TEMP_K and RH_K in Kangnung and the PM_{2.5}_C (0.698; second highest), CO_C, NO₂_C, SO₂_C and PM₁₀_C in Beijing; the other variables have a negative influence. Beijing's measured PM and gas (except O₃_C) significantly contributed to the increase in the predicted SO₂_K(N).

The predicted O₃_K(N) is positively influenced by the measured O₃_K (0.818; highest), TEMP_K (0.525; second highest), WIND_K, PM₁₀_K and PM_{2.5}_K in Kangnung and the O₃_C, SO₂_C, CO_C and PM_{2.5}_C in Beijing, whereas the other variables affect it negatively. The predicted CO_K(N) is positively influenced by the measured CO_K (0.770; highest), RH_K (0.516; second highest), SO₂_K, NO₂_K and PM_{2.5}_K in Kangnung and the NO₂_C, PM_{2.5}_C, CO_C, PM₁₀_C and SO₂_C in Beijing; the other variables affect it negatively. Consequently, after the yellow sand event, five real-time predicted variables (except for the O₃_K(N) case in Kangnung) are positively influenced by all of the PM and gas (except for O₃_C) in Beijing.

Table 7. Partial correlation coefficient matrix of variables to PM₁₀-K(N) in a multivariate regression model at Kangnung after the yellow sand event, 2015.

Pearson Correlation Coefficient (r) after the Yellow Sand Event																
Item	PM ₁₀ -K(N)	PM ₁₀ -K	PM _{2.5} -K	TEMP_K	WIND_K	RH_K	SO ₂ -K	CO_K	O ₃ -K	NO ₂ -K	PM ₁₀ -C	PM _{2.5} -C	SO ₂ -C	CO_C	O ₃ -C	NO ₂ -C
PM ₁₀ -K(N)	1.000	0.888	0.606	0.523	0.036	−0.402	0.377	0.023	0.082	0.444	0.062	0.592	0.503	0.457	−0.278	0.605
PM ₁₀ -K		1.000	0.619	0.532	0.090	−0.437	0.301	−0.081	0.239	0.282	0.066	0.546	0.464	0.430	−0.244	0.527
PM _{2.5} -K			1.000	0.373	−0.187	−0.201	0.623	0.323	−0.030	0.511	0.199	0.803	0.741	0.770	−0.642	0.798
TEMP_K				1.000	0.213	−0.736	0.097	−0.424	0.484	0.341	−0.243	0.419	0.529	0.362	0.202	0.439
WIND_K					1.000	−0.463	−0.213	−0.384	0.365	−0.326	−0.184	−0.242	−0.188	−0.265	0.477	−0.358
RH_K						1.000	−0.099	0.378	−0.488	−0.023	0.289	−0.197	−0.392	−0.271	−0.235	−0.207
SO ₂ -K							1.000	0.689	−0.397	0.572	0.248	0.659	0.631	0.713	−0.568	0.654
CO_K								1.000	−0.724	0.401	0.267	0.327	0.208	0.340	−0.642	0.355
O ₃ -K									1.000	−0.583	−0.199	−0.062	0.111	0.023	0.380	−0.132
NO ₂ -K										1.000	0.085	0.547	0.450	0.389	−0.318	0.639
PM ₁₀ -C											1.000	0.482	0.204	0.255	−0.400	0.234
PM _{2.5} -C												1.000	0.829	0.825	−0.618	0.880
SO ₂ -C													1.000	0.896	−0.484	0.799
CO_C														1.000	−0.658	0.814
O ₃ -C															1.000	−0.726
NO ₂ -C																1.000
Pearson Correlation Coefficient (r) after the Yellow Sand event																
Item	PM _{2.5} -K(N)	PM ₁₀ -K	PM _{2.5} -K	TEMP_K	WIND_K	RH_K	SO ₂ -K	CO_K	O ₃ -K	NO ₂ -K	PM ₁₀ -C	PM _{2.5} -C	SO ₂ -C	CO_C	O ₃ -C	NO ₂ -C
PM _{2.5} -K(N)	1.000	0.618	0.921	0.381	−0.198	−0.161	0.624	0.349	−0.086	0.585	0.221	0.819	0.716	0.732	−0.612	0.807
Pearson Correlation Coefficient (r) after the Yellow Sand event																
Item	NO ₂ -K(N)	PM ₁₀ -K	PM _{2.5} -K	TEMP_K	WIND_K	RH_K	SO ₂ -K	CO_K	O ₃ -K	NO ₂ -K	PM ₁₀ -C	PM _{2.5} -C	SO ₂ -C	CO_C	O ₃ -C	NO ₂ -C
NO ₂ -K(N)	1.000	0.129	0.412	0.334	−0.366	0.050	0.402	0.246	−0.432	0.855	0.034	0.470	0.421	0.355	−0.224	0.564
Pearson Correlation Coefficient (r) after the Yellow Sand event																
Item	SO ₂ -K(N)	PM ₁₀ -K	PM _{2.5} -K	TEMP_K	WIND_K	RH_K	SO ₂ -K	CO_K	O ₃ -K	NO ₂ -K	PM ₁₀ -C	PM _{2.5} -C	SO ₂ -C	CO_C	O ₃ -C	NO ₂ -C
SO ₂ -K(N)	1.000	0.252	0.584	0.072	−0.339	0.023	0.751	0.622	−0.352	0.529	0.250	0.698	0.611	0.679	−0.582	0.662

Table 7. Cont.

Pearson Correlation Coefficient (r) after the Yellow Sand event																
Item	O ₃ _K(N)	PM ₁₀ _K	PM _{2.5} _K	TEMP_K	WIND_K	RH_K	SO ₂ _K	CO_K	O ₃ _K	NO ₂ _K	PM ₁₀ _C	PM _{2.5} _C	SO ₂ _C	CO_C	O ₃ _C	NO ₂ _C
O ₃ _K(N)	1.000	0.403	0.082	0.525	0.449	−0.636	−0.170	−0.536	0.818	−0.420	−0.184	0.028	0.167	0.088	0.286	−0.034
Pearson Correlation Coefficient (r) after the Yellow Sand event																
Item	CO_K(N)	PM ₁₀ _K	PM _{2.5} _K	TEMP_K	WIND_K	RH_K	SO ₂ _K	CO_K	O ₃ _K	NO ₂ _K	PM ₁₀ _C	PM _{2.5} _C	SO ₂ _C	CO_C	O ₃ _C	NO ₂ _C
CO_K(N)	1.000	−0.140	0.283	−0.432	−0.512	0.516	0.455	0.770	−0.615	0.356	0.238	0.340	0.198	0.320	−0.635	0.351

3.5. Scatter Plot and Empirical Regression Formula

Figures 6–8 show scatter plots to display the comparison between the predicted and measured concentrations of PM₁₀, PM_{2.5}, NO₂, SO₂, O₃ and CO calculated by multivariate predictive regression models in Table 2. The scatter plots to test the goodness of the estimations of each variable present a model fitting with the calculated vs. the measured values.

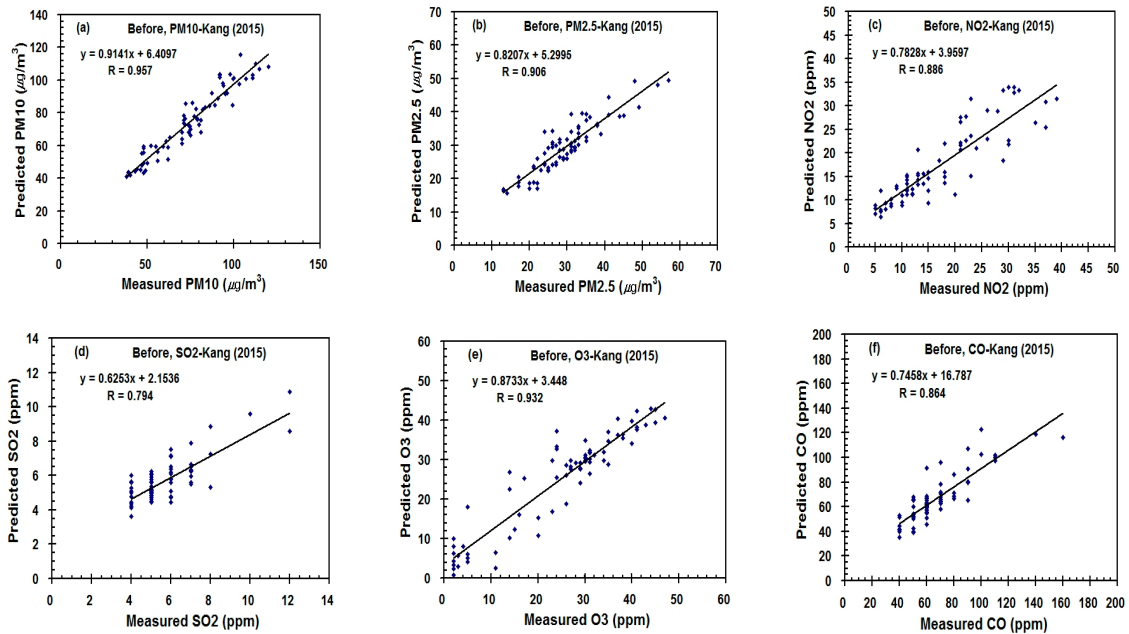


Figure 6. Scatter plots between the measured and predicted concentrations of PM₁₀ (a), PM_{2.5} (b) ($\mu\text{g}/\text{m}^3$) and NO₂ ($\times 1000$) (c), SO₂ ($\times 1000$) (d), O₃ ($\times 1000$) (e), and CO ($\times 100$) (f) (ppm) before the yellow sand event from 21 March to 21 March 2015 in Kangung, Korea.

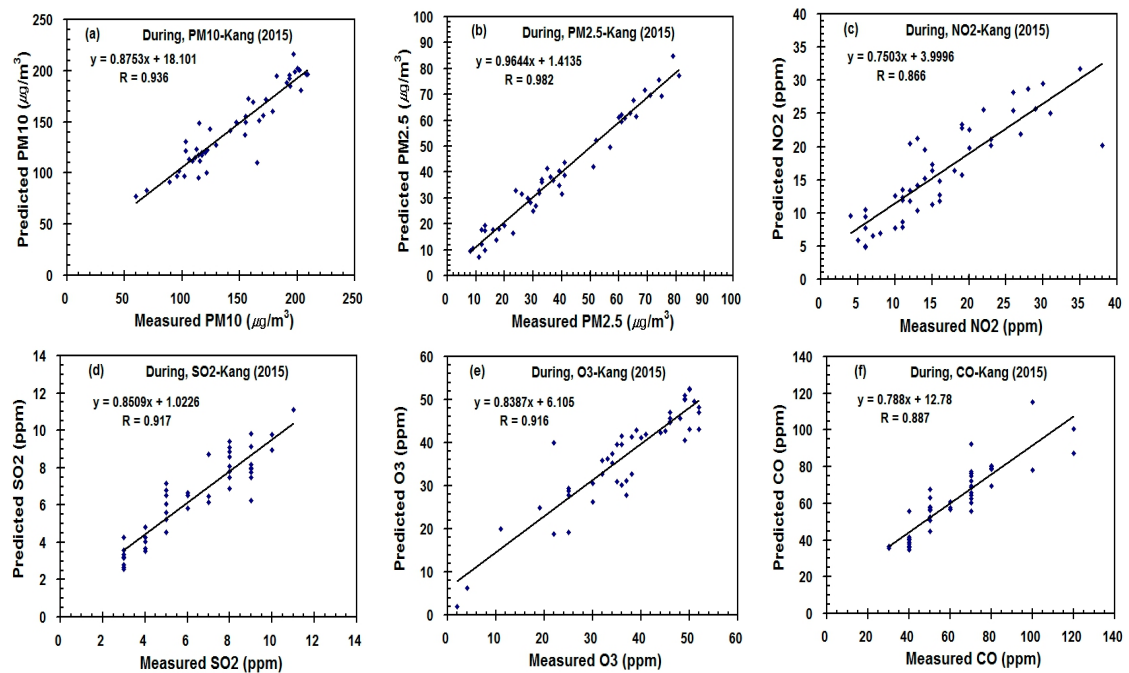


Figure 7. As Figure 6, but for during the event from 21 March to 23 March 2015. PM₁₀ (a), PM_{2.5} (b) ($\mu\text{g}/\text{m}^3$) and NO₂ ($\times 1000$) (c), SO₂ ($\times 1000$) (d), O₃ ($\times 1000$) (e), and CO ($\times 100$) (f) (ppm).

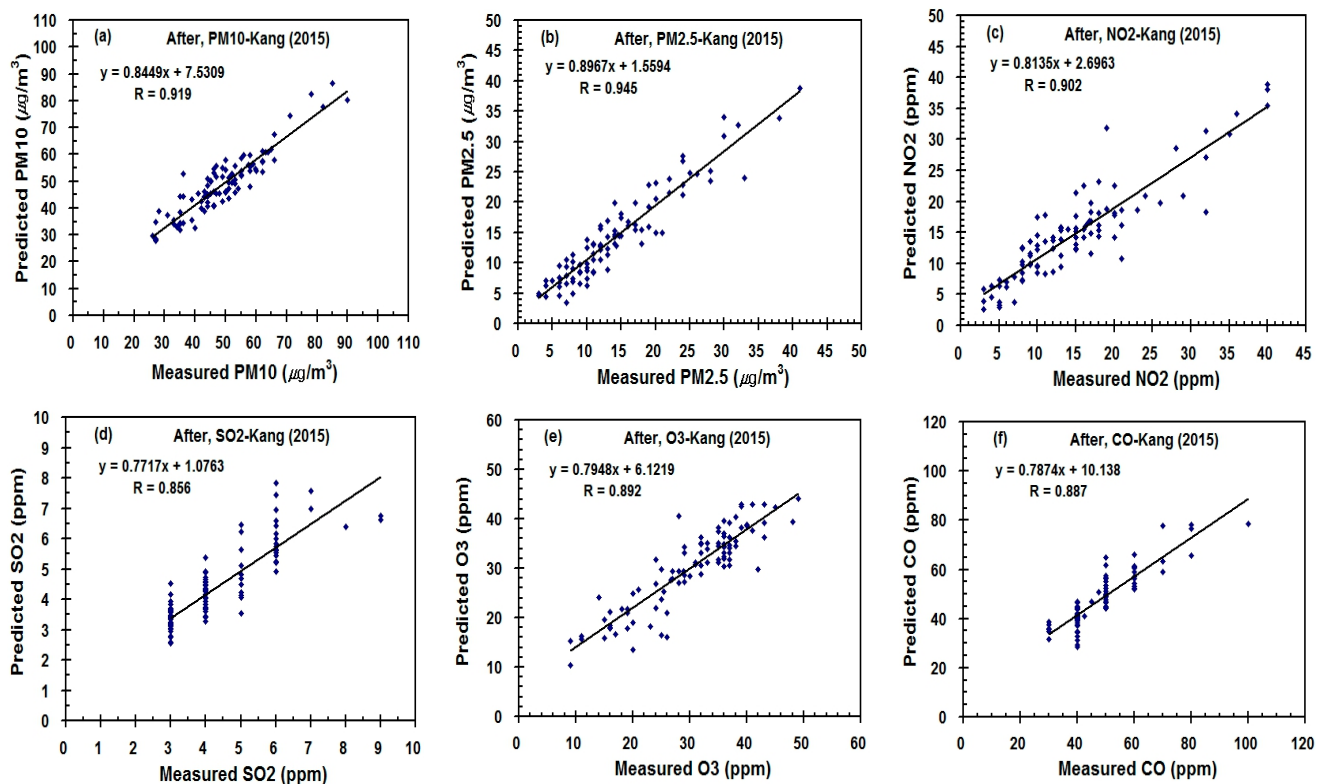


Figure 8. As Figure 6, but for after the event from 23 March to 27 March 2015. PM₁₀ (a), PM_{2.5} (b) ($\mu\text{g}/\text{m}^3$) and NO₂ ($\times 1000$) (c), SO₂ ($\times 1000$) (d), O₃ ($\times 1000$) (e), and CO ($\times 100$) (f) (ppm).

The predicted values for the six hourly variables and their measured values in Figure 6 (as shown in Tables 2–4) are very highly correlated before (0.957, 0.906, 0.886, 0.795, 0.864 and 0.932), during (0.936, 0.982, 0.866, 0.917, 0.887 and 0.916) and after the yellow sand period (0.919, 0.945, 0.902, 0.857, 0.887 and 0.892), respectively. The linear regression equations in the scatter plots can also be easily used to calculate the predicted concentration of each variable from both the three-hours-earlier measured values in Kangnung and two-days-earlier measured values in Beijing.

The scatter plots to test the goodness of the estimations of each variable present a model fitting with the calculated vs. the measured values. The predicted values for the hourly PM₁₀, PM_{2.5}, NO₂, SO₂, O₃ and CO concentrations and their measured values in Figure 6, as shown in Table 2, are very highly correlated before (0.957, 0.906, 0.886, 0.795, 0.864 and 0.932), during (0.936, 0.982, 0.866, 0.917, 0.887 and 0.916) and after the yellow sand period (0.919, 0.945, 0.902, 0.857, 0.887 and 0.892), respectively. The linear regression equations given in the scatter plots can be easily used to calculate the predicted concentration of each variable from both the three-hours-earlier measured values in Kangnung and two-days-earlier measured values in Beijing.

Correlation coefficients between the predicted values and the measured concentrations were very high, over 0.864 for all periods, except for SO₂ (0.795, before), NO₂ (0.866, during) and SO₂ (0.857, after). These empirical regression equations to calculate the predicted values of PM₁₀, PM_{2.5}, NO₂, SO₂, O₃ and CO are very useful and convenient practically and can be used instead of using the multivariate regression equations in Tables 2–4 with three-hours-earlier measured values for each original PM, gas and meteorological element.

3.6. Validation of Multivariate Models

Figure 9 shows that the temporal distribution of the measured (observed) and calculated values for PM₁₀, PM_{2.5}, NO₂, SO₂, O₃ and CO denoted the behavior throughout each period, such as before, during and after the yellow sand periods. These figures display the real-time hourly forecasting values for PM_{10_K(N)}, PM_{2.5_K(N)}, NO_{2_K(N)}, SO_{2_K(N)},

$O_3_K(N)$ and $CO_K(N)$ calculated by multivariate regression models with the three-hours-earlier data before, during and after the yellow sand periods. Through the comparison of the predicted and measured values, we investigated in which time period the applicability of the predicted values to the measured ones was better.

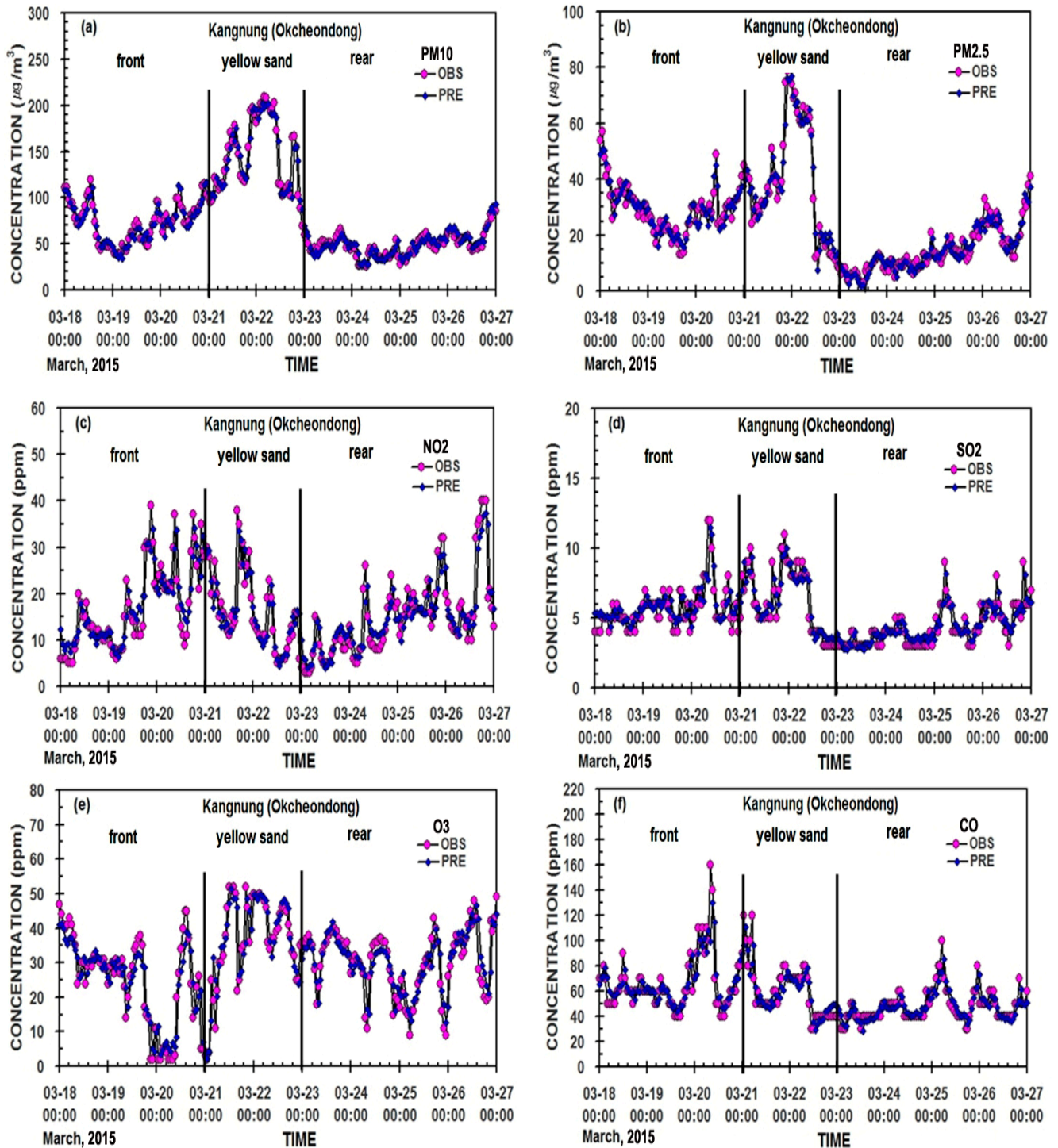


Figure 9. Temporal variations of the measured and real-time predicted values of PM_{10} (a), $PM_{2.5}$ (b) ($\mu\text{g}/\text{m}^3$) and NO_2 ($\times 1000$) (c), SO_2 ($\times 1000$) (d), O_3 ($\times 1000$) (e) and CO ($\times 100$) (f) (ppm) in Kangnung, Korea.

Before the yellow sand period, the difference in the applicability of the real-time predicted values to the measured ones could be shown by the Pearson regression coefficients

of PM₁₀_K(N) (0.957), PM_{2.5}_K(N) (0.906), NO₂_K(N) (0.886), O₃_K(N) (0.932) and CO_K(N) (0.864), which were slightly higher than for SO₂_K(N) (0.795). Therefore, the real-time predicted values of PM₁₀_K(N), PM_{2.5}_K(N), NO₂_K(N), SO₂_K(N), O₃_K(N) and CO_K(N) fit their measured values very well; even the predicted values of SO₂_K(N) were only slightly more deviated from the measured ones.

During the yellow sand event, all of the real-time predicted values fitted the measured values much better than before the event, except for NO₂_K(N), which had a slightly lower correlation coefficient. After the event, the real-time predicted values still fitted with the measured values very well and were similar to the cases before and during the yellow sand period.

As a result, the real-time predicted values of PM₁₀_K(N), PM_{2.5}_K(N), NO₂_K(N), SO₂_K(N), O₃_K(N) and CO_K(N) were all very close to their measured values, showing that they were reproduced well, even though the applicability of SO₂_K(N) was slightly more deviated before the yellow sand event. This means that there is a time gap between their concentrations or it has a slightly bigger or smaller value in the higher and the maximum concentrations before the period. This may be attributed to a slightly lower correlation coefficient, as shown in Figure 6 and Table 2.

We further compared our simulation results using multivariate regression models and artificial neural network models with similar scientific works by several scientists in Table 8. As hourly averaged or daily averaged pollutant concentrations with or without meteorological data were used differently by individual scientists, it is not easy to compare the results calculated by each other. However, even though the same kinds of input data for the model were used, it is desirable to compare the accuracy of the different model performances.

Thus, the comparison results in Table 8 show that the correlation coefficients between the hourly predicted and measured values calculated by our multivariate regression models were 0.886 to 0.982. The accuracy of our calculated values is in the middle range compared with the results calculated using various models by other authors. If the performance of our multivariate regression model using hourly averaged input data is compared with the model performance by ANN-sig, SVR, random forest and multivariate regression using daily averaged data, it has much higher accuracy of calculation than the models performed by Jeon and Son [36] and Kim [37]; however, our model performance has relatively lower accuracy than Lim's models. Our future research will be carried out using both artificial neural network models and multivariate regression models and the calculation results from the models will be compared with each other.

Table 8. Prediction performance using different models from different scientists regarding the yellow sand event (YS), with correlation coefficients (Pearson's r). Reference: ANN-sig (Artificial neural network-sigmoid), ANN-tanh (Artificial neural network-tanh), SVM (Support vector machine), RF (Random forest), Multivariate (Multivariate regression) and SVR (Support vector regression).

Name	Model	Pearson r											
		Before (Hourly) YS			During (Hourly) YS			After (Hourly) YS			Daily/Seasonal/ Annual		
		PM ₁₀	PM _{2.5}	NO ₂	PM ₁₀	PM _{2.5}	NO ₂	PM ₁₀	PM _{2.5}	NO ₂	PM ₁₀	PM _{2.5}	NO ₂
(1) Jeon and Son, 2018 [40]	ANN-sig												0.737
	SVM												0.751
	Random F												0.726
(2) Kim, 2019 [37]	Multivariate												0.849
(3) Lim, 2019 [38]	ANN-sig												0.962
	SVR												0.962
	Multivariate												0.958
(4) Choi and Choi, 2021 [41]	Multivariate	0.983	0.998		0.916	0.998		0.941	0.998				
(5) Choi, S.-M., 2022 [39]	ANN-sig	0.954	0.866	0.873	0.941	0.960	0.975	0.930	0.953	0.917			
	ANN-tanh	0.974	0.958	0.953	0.971	0.983	0.930	0.953	0.960	0.959			
	Multivariate	0.961	0.909	0.896	0.948	0.977	0.875	0.920	0.947	0.903			
(6) Choi et al., 2023	Multivariate	0.957	0.906	0.886	0.936	0.982	0.866	0.919	0.945	0.902			

4. Conclusions

Predicting real-time air pollution concentrations in a city using historical air pollution concentration data is a very important but difficult task in all industrialized countries. The reason is that too many factors are involved and some of the air pollutants cross the border and flow into the local city, making the air pollution concentration in that city very high and the air pollution concentration also depends on the weather conditions of the city itself. In this study, we developed multivariate regression models for the real-time prediction of air quality at the current time before, during and after the yellow sand periods in Kangnung using the 3 h-earlier PM and gas concentration and meteorological parameter data from the city and the 2-days-earlier PM and gas concentration data from Beijing. Our research results are summarized as follows.

The correlation coefficient between the predicted and measured real-time PM₁₀ and PM_{2.5} values calculated by the model were 0.919–0.957 and 0.906–0.945, and the prediction abilities during the event were the maximum. On the other hand, the correlation coefficients for NO₂, SO₂, O₃ and CO were 0.866–0.902, 0.795–0.917, 0.892–0.932 and 0.864–0.887, respectively, which were slightly lower than those for the PM values. However, their predicted values well reflect the measured ones and the predictive performance of our models was slightly better than other scholars' multivariate regression models.

Before the Yellow Sand event, the PM₁₀, PM_{2.5}, NO₂, SO₂ and CO concentrations in Kangnung were not affected by the PM concentrations in Beijing, but some of them were affected by the gas concentrations in Beijing. During and after the yellow sand event, all PM and gas concentrations, except for O₃, in Kangnung City were affected by all PM and gas concentrations in Beijing City, except for O₃. The contribution of meteorological parameters to air pollutant concentrations in Kangnung was relatively smaller than the effect of PM and gas concentrations in Beijing City. The significance levels of all correlation coefficients were less than 0.001, indicating that they were very significant.

Generally, to predict air pollution concentrations, numerical models, multivariate regression statistical models, neural network models and meteorological satellite image interpretation methods are used. Since each method has advantages and disadvantages and the methods complement each other, I think that there is no need to analyze which method is superior. Rather, there is a need to improve each process to improve the prediction ability. Further studies of air pollution prediction in urban areas need to obtain a deeper, more comprehensive understanding the physical processes leading to the observed differences between local cities and trans-border cities for solving the nationwide air quality problem via useful models.

Author Contributions: Conceptualization, S.-M.C. and H.C.; methodology, S.-M.C., H.C. and W.P.; software, S.-M.C. and H.C.; validation, S.-M.C., H.C. and W.P.; formal analysis, S.-M.C. and H.C.; investigation, S.-M.C. and H.C.; resources, S.-M.C. and H.C.; data curation, S.-M.C. and H.C.; writing—original draft preparation, S.-M.C. and H.C.; writing—review and editing, H.C. and S.-M.C.; visualization, S.-M.C.; supervision, H.C. and W.P.; project administration, H.C.; funding acquisition, H.C. All authors have read and agreed to the published version of the manuscript.

Funding: This research received no external funding.

Data Availability Statement: The hourly PM₁₀, PM_{2.5}, SO₂, CO, O₃ and NO₂ concentrations measured at the Okchandong observation point of Kangnung city by the Gangwon Health and Environmental Research Institute were obtained from the homepage (Air Korea) of the Korea Environment Corporation using the website address <https://www.airkorea.or.kr/web/>, accessed on 10 January 2021. The hourly meteorological data (air temperature, wind speed and relative humidity) measured at the Okchandong observation point close to Kangnung city by Gangwon Regional Meteorological Administration, Korea can be obtained from the Korea Meteorological Administration (KMA) through the website address <https://data.kma.go.kr/>, accessed on 1 February 2023. The hourly particulate matter (PM₁₀ and PM_{2.5}) and gas (SO₂, CO, O₃ and NO₂) data measured at the Yongdingmen observation point of Beijing city (China) can be acquired through internet using the website addresses <https://quotsoft.net/air/> or <http://www.bjmemc.com.cn/>.

Acknowledgments: The authors (S.-M.C., H.C. and W.P.) express many thanks to the KMA for the meteorological data and to the Beijing Municipal Ecological and Environmental Monitoring Center for air quality data in the Beijing district that was used in this work.

Conflicts of Interest: The authors declare no conflict of interest.

References

1. Gao, Y.; Anderson, J.R. Characteristics of Chinese aerosols determined by individual particle analysis. *J. Geophys. Res.* **2001**, *106*, 18037–18045. [[CrossRef](#)]
2. Lee, S.C.; Cheng, Y.; Ho, K.F.; Cao, J.J.; Loui, P.K.K.; Chow, J.C.; Watson, J.G. PM₁₀ and PM_{2.5} characteristics in the roadside environment of Hong Kong. *Aerosol Sci. Technol.* **2006**, *40*, 157–165. [[CrossRef](#)]
3. Zhao, S.; Yu, Y.; Yin, D.; He, J.; Liu, N.; Qu, J.; Xiao, J. Annual and diurnal variations of gaseous and particulate pollutants in 31 provincial spatial cities based on in sit air quality monitoring data from China National Environmental Monitoring Center. *Environ. Int.* **2016**, *86*, 92–106. [[CrossRef](#)]
4. Ma, X.; Jia, H. Particulate matter and gaseous pollutions in three megacities over China: Situation and implication. *Atmos. Env.* **2016**, *140*, 476–494. [[CrossRef](#)]
5. Xiao, K.; Wang, Y.K.; Wu, G.; Fu, B.; Zhu, Y. Spatiotemporal characteristics of air pollutions (PM₁₀, PM_{2.5}, SO₂, NO₂, O₃, and CO) in the inland basin city of Chengdu, Southwest China. *Atmosphere* **2018**, *9*, 74. [[CrossRef](#)]
6. Li, C.; Dai, Z.; Yang, L.; Ma, Z. Spatiotemporal characteristics of air quality across Weifang from 2014–2018. *Int. J. Environ. Res. Public Health* **2019**, *16*, 3122. [[CrossRef](#)]
7. Chow, J.C. Health effects of fine particulate air pollution; Lines that connect. *J. Air Waste Manag. Assoc.* **2006**, *56*, 707–708. [[CrossRef](#)]
8. Huang, D.; Xu, J.; Zhang, S. Valuing the health risks of particulate air pollution in the Pearl River Delta, China. *Environ. Sci. Policy* **2012**, *15*, 38–47. [[CrossRef](#)]
9. Li, F.; Liu, Y.; Lu, J.J.; Liang, L.; Harmer, P. Ambient air pollution in China poses a multi-faced health threat to outdoor physical activity. *J. Epidemiol. Community Health* **2015**, *69*, 201–204. [[CrossRef](#)]
10. Shen, F.; Ge, X.; Hu, J.; Nie, D.; Tian, L.; Chen, M. Air pollution characteristics and health risks in Henan Province, China. *Environ. Res. Sci.* **2017**, *156*, 625–634. [[CrossRef](#)]
11. He, J.Q.; Yu, X.N.; Zhu, B.; Yuan, L.; Ma, J.; Shen, L.; Zhu, J. Characteristics of aerosol extinction and low visibility in haze weather in winter of Nanjing, China. *Environ. Sci.* **2016**, *36*, 1645–1653.
12. Kim, Y.J.; Kim, K.W.; Kim, S.D.; Lee, B.K.; Han, J.S. Fine particulate matter characteristics and its impact on visibility impairment at two sites in Korea: Seoul and Incheon. *Atmos. Environ.* **2000**, *40*, 593–609. [[CrossRef](#)]
13. Sun, J.; Zhang, M.; Liu, T. Spatial and temporal characteristics of dust storms in China and its surrounding regions, 1960–1999: Relations to source area and climate. *J. Geophys. Res.* **2001**, *106*, 325–10333. [[CrossRef](#)]
14. Darmenova, K.; Sokolik, I.N.; Darmenov, A. Characterization of east Asian dust outbreaks in the spring of 2001 using ground-based and satellite data. *J. Geophys. Res.* **2005**, *110*, D02204. [[CrossRef](#)]
15. Wang, X.; Ma, Y.; Chen, H.; Wen, G.; Chen, S.; Tao, Z.; Chung, Y. The relation between sandstorms and strong winds in Xinjiang, China. *Water Air Soil Pollut. Focus* **2003**, *3*, 67–79. [[CrossRef](#)]
16. Uno, I.; Carmichael, G.R.; Streets, D.G.; Yang, Y.; Yienger, J.J.; Satake, S.; Wang, Z.; Woo, J.H.; Guttikunda, S.; Uematsu, M.; et al. Regional chemical weather forecasting system CFORS: Model descriptions and analysis of surface observations at Japanese island stations during the ACE-Asia experiment. *J. Geophys. Res.* **2003**, *108*, 8668. [[CrossRef](#)]
17. Choi, H.; Zhang, Y.H. Predicting duststorm evolution with vorticity theory. *Atmos. Res.* **2008**, *89*, 338–350. [[CrossRef](#)]
18. Iwasaka, Y.; Shibata, T.; Nagatani, T.; Shi, G.-Y.; Kim, Y.S.; Matsuki, A.; Trochkin, D.; Zhang, D.; Yamada, M.; Nagatani, M.; et al. Large depolarization ratio of free tropospheric aerosols over the Taklamakan desert revealed by lidar measurements: Possible diffusion and transport of dust particles. *J. Geophys. Res.* **2003**, *108*, 8652. [[CrossRef](#)]
19. Gao, T.; Su, L.; Ma, Q.; Li, H.; Yu, X. Climate analyses on increasing dust storm frequency in the springs of 2000 and 2001 in Inner Mongolia. *Int. J. Climatol.* **2003**, *23*, 1743–1755. [[CrossRef](#)]
20. Sun, J. Provenance of loess material and formation of deposits on the Chinese Loess Plateau. *Earth Planet. Sci. Lett.* **2002**, *203*, 845–859. [[CrossRef](#)]
21. Chung, Y.S.; Kim, H.S.; Natsagdorj, L.; Jugder, D.; Chen, S.J. On yellow sand occurred during 1997–2000. *J. Korean Meteor. Soc.* **2001**, *37*, 305–316. [[CrossRef](#)]
22. Zhang, X.Y.; Gong, S.L.; Shen, Z.X.; Mei, F.M.; Xi, X.X.; Liu, L.C.; Zhou, Z.J.; Wang, D.; Wang, Y.Q.; Cheng, Y. Characteristics of soil dust, aerosol in China in its transport and distribution during 2001 ACE-Asia: 1: Network observations. *J. Geophys. Res.* **2003**, *108*, 4261. [[CrossRef](#)]
23. He, Z.; Kim, Y.J.; Ogunjobi, O.; Hong, C.S. Characteristics of PM_{2.5} species and long-range transport of air masses at Taeanback ground station, South Korea. *Atmos. Environ.* **2003**, *37*, 219–230. [[CrossRef](#)]
24. Kim, K.W.; Kim, Y.J.; Oh, S.J. Visibility impairment during Yellow Sand periods in the urban atmosphere of Kwangju, Korea. *Atmos. Environ.* **2001**, *35*, 5157–5167. [[CrossRef](#)]

25. Shim, K.; Kim, M.-H.; Lee, H.-J.; Nishizawa, T.; Shimizu, A.; Kobayashi, H.; Kim, C.-H.; Kim, S.-W. Exacerbation of PM_{2.5} concentration due to unpredictable weak Asian dust storm: A case study of an extraordinarily long-lasting spring haze episode in Seoul, Korea. *Atmos. Environ.* **2022**, *287*, 119261. [[CrossRef](#)]
26. Lin, T.H. Long-range transport of yellow sand to Taiwan in spring 2000: Observed evidence and simulation. *Atmos. Environ.* **2001**, *35*, 5873–5882. [[CrossRef](#)]
27. Uno, I.; Amano, H.; Emori, S.; Kinoshita, K.; Matsui, I.; Sugimoto, N. Trans-Pacific yellow sand transport observed in April, 1998: A numerical simulation. *J. Geophys. Res.* **2001**, *106*, 18331–18344. [[CrossRef](#)]
28. Chin, M.; Ginoux, P.; Lucchesi, R.; Huebert, B.; Weber, R.; Anderson, T.; Masonis, S.; Blomquist, B.; Bandy, A.; Thomson, D. A global aerosol model forecast for the ACE-Asia field experiment. *J. Geophys. Res.* **2003**, *108*, 8654. [[CrossRef](#)]
29. Jaffe, D.; McKendry, I.; Anderson, T.; Price, H. Six "new" episodes of trans-Pacific transport of air pollutants. *Atmos. Environ.* **2003**, *37*, 391–404. [[CrossRef](#)]
30. McKendry, I.G.; Hacker, J.P.; Stull, R.; Sakiyama, S.; Mignacca, D.; Reid, K. Long-range transport of Asian dust to the lower Fraser Valley, British Columbia, Canada. *J. Geophys. Res.* **2001**, *106*, 18361–18370. [[CrossRef](#)]
31. Lee, M.S.; Chung, J.D. Impact of yellow dust transport from Gobi Desert on fractional ratio and correlations of temporal PM₁₀, PM_{2.5} and PM₁ at Gangneung city. *J. Environ. Sci.* **2012**, *21*, 217–231. [[CrossRef](#)]
32. Bhaskar, B.V.; Mehta, V.M. Atmospheric particulate pollutants and their relationship with meteorology in Ahmedabad. *Aerosol. Air Qual. Res.* **2010**, *10*, 301–315. [[CrossRef](#)]
33. Cheng, Y.; He, K.B.; Du, Z.Y.; Zheng, M.; Duan, F.K.; Ma, Y.L. Humidity plays an important role in the PM_{2.5} pollution in Beijing. *Environ. Pollut.* **2015**, *197*, 68–75. [[CrossRef](#)] [[PubMed](#)]
34. Li, X.; Ma, Y.; Wang, Y.; Liu, N.; Hong, Y. Temporal and spatial analysis of particulate matter (PM₁₀ and PM_{2.5}) and its relationship with meteorological parameters over an urban city in northeast China, 2017. *Atmos. Res.* **2017**, *198*, 185–193. [[CrossRef](#)]
35. Shi, C.; Yuan, R.; Wu, B.; Meng, Y.; Zhang, H.; Zhang, H.; Gong, Z. Meteorological conditions to PM_{2.5} pollution in winter 2016/2017 in the western Yangtze delta, China. *Sci. Total Environ.* **2018**, *642*, 1221–1232. [[CrossRef](#)]
36. Zhao, D.; Chen, H.; Yu, E.; Luo, T. PM_{2.5}/PM₁₀ ratios in eight economic regions and their relationship with meteorology in China. *Adv. Meteorol.* **2019**, 5295726. [[CrossRef](#)]
37. Kim, M.J. The effects of transboundary air pollution from China on ambient air quality in South Korea. *Heliyon* **2019**, *5*, e06283. [[CrossRef](#)]
38. Lim, J.-M. An estimation model of fine dust concentration using meteorological environment data and machine learning. *J. Inform. Technol.* **2019**, *18*, 173–185.
39. Choi, S.-M. Implementation of Prediction System on Urban Air Quality Using Artificial Neural Network and Multivariate Regression Models during the COVID-19 Pandemic and Yellow Dust Event. Ph.D. Thesis, Konkuk University, Seoul, Republic of Korea; pp. 1–268.
40. Jeon, S.; Son, Y.S. Prediction of fine dust PM₁₀ using a deep neural network model. *Korean J. Appl. Stat.* **2018**, *31*, 205–285.
41. Choi, S.-M.; Choi, H. Statistical modeling for PM₁₀, PM_{2.5}, and PM₁ at Gangneung affected by local meteorological variables and PM₁₀ and PM_{2.5} at Beijing for non- and dust periods. *App. Sci.* **2021**, *11*, 11958. [[CrossRef](#)]
42. Mendez, M.R.; Souto, J.A.; Vila-Guerau de Arellano, J.; Lucas, T.; Casares, J.J. Dispersion and transformation of nitrogen oxides emitted from a point source. *WIT Trans. Ecol. Environ.* **1997**, *19*, 10.
43. Chu, B.; Zhang, S.; Liu, J.; Ma, Q.; He, H. Significant concurrent decrease in PM_{2.5} and NO₂ concentrations in China during COVID-19 epidemic. *J. Environ. Sci.* **2021**, *99*, 346–353. [[CrossRef](#)] [[PubMed](#)]

Disclaimer/Publisher's Note: The statements, opinions and data contained in all publications are solely those of the individual author(s) and contributor(s) and not of MDPI and/or the editor(s). MDPI and/or the editor(s) disclaim responsibility for any injury to people or property resulting from any ideas, methods, instructions or products referred to in the content.